ORNL/TM-5528

Electromechanical Stress Analysis of Transversely Isotropic Solenoids

W. H. Gray
J. K. Ballou

MASTER

OAK RIDGE NATIONAL LABORATORY
OPERATED BY UNION CARBIDE CORPORATION FOR THE ENERGY RESEARCH AND DEVELOPMENT ADMINISTRATION

BLANK PAGE

Printed in the United States of America. Available from
National Technical Information Service
U.S. Department of Commerce
5285 Port Royal Road, Springfield, Virginia 22161
Price: Printed Copy $4.50; Microfiche $3.00

ORNL/TM-5528

Contract No. W-7405-eng-26

Fusion Energy Division

ELECTROMECHANICAL STRESS ANALYSIS OF TRANSVERSELY ISOTROPIC SOLENOIDS

W. H. Gray

J. K. Ballou

(Submitted for publication in Journal of Applied Physics)

NOTICE This document contains information of preliminary nature. It is subject to revision or correction and therefore does not represent a final report.

Date Published - March 1977

Prepared by the
OAK RIDGE NATIONAL LABORATORY
Oak Ridge, Tennessee 37830
operated by
UNION CARBIDE CORPORATION
for the
ENERGY RESEARCH AND DEVELOPMENT ADMINISTRATION

CONTENTS

ELECTROMECHANICAL STRESS ANALYSIS OF TRANSVERSELY ISOTROPIC SOLENOIDS*

W. H. Gray and J. K. Ballou
Magnetics and Superconductivity Section
Fusion Energy Division
Oak Ridge National Laboratory
Oak Ridge, Tennessee 37830

ABSTRACT

The mechanical behavior of superconducting magnets deviates from isotropy due to their construction techniques, which involve layering superconductor, insulation, and sometimes structural reinforcement within the windings. Previous mechanical analyses considered the windings of a magnet to behave isotropically. This paper describes an analytical solution for the deflection, stress, and strain of axisymmetric, electromechanically loaded, and rotationally transversely isotropic solenoids. The results indicate that for magnets with a large radial build compared to inner radius, transverse isotropy has a dramatic effect upon the mechanical response to load; for magnets with a small radial build compared to inner radius, transverse isotropy has a negligible effect.

*Research sponsored by the Energy Research and Development Administration under contract with Union Carbide Corporation.

I. INTRODUCTION

An extensive effort is presently being undertaken to design and construct large, high field superconducting magnets for use in magnetic fusion energy research, energy storage devices, and related systems. An important part of this effort is directed toward the evaluation of stresses and deformations in electromagnets caused by the application of electromechanical body forces, differential temperatures, winding preloads, and other forces. This report concerns one aspect of this evaluation — namely the stress analysis of transversely isotropic, axisymmetric, electromechanically loaded solenoids.

A number of analytical solutions are available to determine the electromechanical stresses induced in a magnet constructed with homogeneous, isotropic materials and loaded axisymmetrically assuming a condition of plane stress. Lontai and Marston[1] were the first to use classical elasticity to derive equations for displacement, stresses, and strains in a solenoid, assuming a linear dependence of the axial magnet field with the radius. Similar equations have been independently derived by Westendorp and Kilb[2] and by Burkhard.[3] Kuznetson[4] and Leon[5] have derived similar solutions considering more complex approximations to the axial magnetic field at the solenoid midplane. Johnson[6] has extended these solutions to consider a piecewise linear axial magnetic field approximation in a computer code called "STANSOL." This computer code includes consideration of currents, axial magnetic fields, differential temperature, and winding preload which may vary arbitrarily from layer to layer throughout the coil.

The STANSOL program, described more fully in Refs. 7 and 8, uses a solution in which the coil is initially assumed to be a series of independent, thick-walled cylindrical layers to which loads are applied. nonhomogeneous cylinder by establishing displacement compatibility between layers. After determination of the layer-to-layer interface pressures required to establish this displacement compatibility, it is possible to compute all desired stresses and deformations in the coil.

A superconducting composite wire is not isotropic and a solenoid made of this material will behave orthotropically. Further, if insulating materials or reinforcing structure or both are introduced into the winding, then a magnet will behave in a more orthotropic manner. Section 2 of this report defines a model for the behavior of a transversely isotropic superconducting solenoid. (Novitskii and Shaktarin[9] derive a similar model but do not present a solution.) A transversely isotropic material is a special case of an orthotropic material where there are only two independent orthogonal material planes instead of three. A discussion of transverse isotropy as it applies to a superconducting composite wire is presented by Gray and Sun.[10] A solution is presented for the special case of a constant current, axisymmetric solenoid with a linearly varying axial magnetic field.

In Sec. 3, several example solutions are presented which illustrate the effects of low modulus insulation, high modulus reinforcement, or both being included within the windings. In Sec. 4, we estimate the error involved in making the linear axial magnetic field approximation, which is an indication of whether a more exact solution for the electromechanical behavior should be performed. Finally, in Sec. 5, several contour plots of constant values of maximum hoop stress are presented as functions of solenoid geometry and transverse isotropy from which one can rapidly estimate the level of electromechanical stress in a solenoid.

II. THEORETICAL DEVELOPMENT OF THE ELECTROMECHANICAL EQUILIBRIUM EQUATION FOR AXISYMMETRIC TRANSVERSELY ISOTROPIC SOLENOIDS

In this section we derive and solve the electromechanical equilibrium equation for a solenoid using the classical theory of elasticity. The plane stress equilibrium, constitutive, and kinematic equations are presented as they apply to an axisymmetric solenoid with transversely isotropic material properties.

A. Stress Equilibrium Equation

The stress equilibrium equation in polar coordinates for a homogeneous axisymmetric body in a condition of plane stress under the influence of a radial body force per unit volume, F_R, is

$$\sigma_R - \sigma_\theta + R\frac{d\sigma_R}{dR} + RF_R = 0 \quad , \tag{1}$$

where R is the radial coordinate, σ_R is the radial stress, and σ_θ is the hoop or tangential stress (see Fig. 1).

B. Electromechanical Body Force

In a solenoid the interaction of the current and the magnetic field produces a Lorentz body force (force per unit volume). This body force is the only one considered in this analysis and it can be calculated from

$$\vec{F} = \vec{j} \times \vec{B} \quad , \tag{2}$$

where $\vec{j}$ is the current density vector and $\vec{B}$ is the magnetic field vector.

For this axisymmetric problem the current is considered to flow uniformly and tangentially (see Fig. 1), and therefore $\vec{j}$ possesses only one vectorial component,

$$\vec{j} = j\ (\hat{i}_\theta) \quad , \tag{3}$$

where j is the constant current density and $\hat{i}_\theta$ is a tangential unit vector in polar coordinates. At the midplane of a solenoid, the magnetic field produced by such a current density can have only an axial component,

$$\vec{B} = B_z\ (\hat{i}_z) \quad , \tag{4}$$

where $\hat{i}_z$ is a polar coordinate axial unit vector and B_z is the axial magnetic field which is a function of radial position.

Using Eqs. (3) and (4) in Eq. (2), the radial electromechanical body force per unit volume is

$$F_R = jB_z\ (\hat{i}_r) \quad . \tag{5}$$

Substituting Eq. (5) into Eq. (1), the equation governing stress equilibrium for a two-dimensional, homogeneous axisymmetric solenoid in a plane-stress condition is

$$\sigma_R - \sigma_\theta + R\,\frac{d\sigma_R}{dR} + jB_zR = C \quad . \tag{6}$$

C. The Material Constitutive Relationships

The stresses are related to the strains by the material constitutive relationships. For an elastic orthotropic material in a state of plane-stress the constitutive equations are[11]

$$\sigma_R = \left[\frac{E_\theta}{n - \nu_{\theta R}^2}\right]\left(\varepsilon_R + \nu_{\theta R}\,\varepsilon_\theta\right) \quad , \tag{7}$$

$$\sigma_\theta = \left[\frac{E_\theta}{n - \nu_{\theta R}^2}\right]\left(n\varepsilon_\theta + \nu_{\theta R}\,\varepsilon_R\right) \quad , \tag{8}$$

and

$$n = E_\theta / E_R \quad , \tag{9}$$

where E_θ is Young's modulus associated with the hoop direction, E_R is Young's modulus associated with the radial direction, $\nu_{\theta R}$ is the Poisson ratio coupling the radial direction and hoop direction,[12] and ϵ_r and ϵ_θ are the radial and hoop strains, respectively. The coordinate system in Fig. 1 illustrates that circumferential application of Eqs. (7) and (8) does not violate the axisymmetric condition, as neither of these equations is dependent upon angular position. This situation is referred to as transverse isotropy[13] and implies that these material properties are invariant within this coordinate system, which would not be the case if a Cartesian coordinate system had been chosen as a reference.

D. The Strain Displacement Relationships

For this axisymmetric, plane-stress analysis the kinematic equations which relate strain and deflection are

$$\epsilon_R = \frac{u}{R} \tag{10}$$

and

$$\epsilon_\theta = \frac{du}{dR} \quad , \tag{11}$$

where u is the radial displacement.

Combination of Eqs. (6) through (11) yields the following second order, first degree, linear, nonhomogeneous, ordinary differential equation for the radial displacement:

$$\frac{d^2u}{dR^2} + \frac{1}{R}\frac{du}{dR} - n\frac{u}{R^2} = \frac{-jB_z}{E_\theta}(n - \nu^2_{\theta R}) \ . \tag{12}$$

E. Solution For The Radial Displacement

Defining γ as the nondimensional radius, R/R_i, where R_i is equal to the inner radius, Eq. (12) can be normalized to

$$\frac{d^2u}{d\gamma^2} + \frac{1}{\gamma}\frac{du}{d\gamma} - n\frac{u}{\gamma^2} = \frac{-jB_z R_i^2 (n - \nu^2_{\theta R})}{E_\theta} \ . \tag{13}$$

If the axial magnetic field is assumed to be a linear function of radial position, then

$$B_z = B_i\ [1 + b\ (\gamma - 1)] \tag{14}$$

where

$$b = \frac{B_o - B_i}{B_i\ (\alpha - 1)} \tag{15}$$

and

$$\alpha = R_o/R_i. \tag{16}$$

R_i and R_o are the inner and outer radii of the solenoid, and B_i and B_o are the axial magnetic field strengths at the inner and outer radial positions, respectively.

Substituting the assumed magnetic field distribution into Eq. (13) yields

$$\frac{d^2u}{d\gamma^2} + \frac{1}{\gamma}\frac{du}{d\gamma} - n\frac{u}{\gamma^2} = \frac{-\xi}{\zeta}\left[1 + b\ (\gamma - 1)\right] \tag{17}$$

where

$$\xi = jB_iR_i \tag{18}$$

and

$$\zeta = \frac{E_\theta}{(n - \nu_{\theta R}^2)R_i} \ . \tag{19}$$

Equation (17) is the form of Cauchy's equation[14] and therefore has a complementary solution, u_c, of the form

$$u_c = C_1\gamma^{\sqrt{n}} + C_2\gamma^{-\sqrt{n}} \tag{20}$$

where C_1 and C_2 are undetermined coefficients. The particular solution, u_p, to Eq. (17) is

$$u_p = \frac{-\xi}{\zeta}\left[\frac{(1-b)}{(4-n)}\gamma^2 + \frac{b\gamma^3}{(9-n)}\right] . \tag{21}$$

Combination of Eqs. (20) and (21) gives the complete solution in terms of the two unknown coefficients.

If the solenoid is unsupported, then its radial stress at the inner and outer surfaces of the coil must be zero. These boundary conditions stated mathematically are

$$\sigma_R = 0 \text{ at } \gamma = 1$$

and

$$\sigma_R = 0 \text{ at } \gamma = \alpha \quad .$$

Substituting Eqs. (20) and (21) into the radial constitutive relationship, Eq. (7) while imposing the above boundary conditions gives two simultaneous linear equations for the determination of C_1 and C_2. Solving for these constants yields

$$C_1 = \frac{\xi}{\zeta}\left[\frac{1}{(\nu_{\theta R} + \sqrt{n})(\alpha^{2\sqrt{n}} - 1)}\right]\left[\frac{(\nu_{\theta R} + 2)(1 - b)(\alpha^{\sqrt{n} + 2} - 1)}{(4 - n)}\right.$$

$$\left. + \frac{(\nu_{\theta R} + 3)b(a^{\sqrt{n} + 3} - 1)}{(9 - n)}\right] \tag{22}$$

and

$$C_2 = \frac{\xi}{\zeta}\left[\frac{\alpha^{2\sqrt{n}}}{(\sqrt{n} - \nu_{\theta R})(a^{2\sqrt{n}}-1)}\right]\left[\frac{(\nu_{\theta R} + 2)(1 - b)(a^{2-\sqrt{n}}-1)}{(4 - n)}\right.$$

$$\left. + \frac{(\nu_{\theta R} + 3)b(a^{3-\sqrt{n}}-1)}{(9 - n)}\right] . \qquad (23)$$

The solution for radial displacement is then

$$u = C_1\gamma^{\sqrt{n}} + C_2\gamma^{-\sqrt{n}} - \frac{\xi\gamma^2}{\zeta}\left[\frac{(1 - b)}{(4 - n)} + \frac{b\gamma}{(9 - n)}\right] . \qquad (24)$$

F. Equations for Radial and Hoop Strain

The equations for radial and hoop strain can be obtained by substitution of Eq. (24) into the kinematic relations, Eqs. (10) and (11):

$$\varepsilon_r = \frac{1}{R_i}\left\{C_1\sqrt{n}\gamma^{(\sqrt{n}-1)} - C_2\sqrt{n}\gamma^{-(\sqrt{n}+1)} \frac{-\xi\gamma}{\zeta}\left[\frac{2(1 - b)}{(4 - n)} + \frac{3b\gamma}{(9 - n)}\right]\right\} \qquad (25)$$

and

$$\varepsilon_\theta = \frac{1}{R_i}\left\{C_1\gamma^{(\sqrt{n} - 1)} + C_2\gamma^{-(\sqrt{n} + 1)} - \frac{\xi\gamma}{\zeta}\left[\frac{(1 - b)}{(4 - n)} - \frac{b\gamma}{(9 - n)}\right]\right\} . \qquad (26)$$

G. Equations for Radial and Hoop Stress

The equations for radial and hoop stress can be obtained by substitution of Eqs. (25) and (26) into the constitutive relations, Eqs. (7) and (8):

$$\frac{\sigma_\theta}{jB_iR_i} = \frac{(\nu_{\theta R} + 2)(1 - b)}{(4-n)(\alpha^{2\sqrt{n}}-1)} \Bigg\{ [\alpha^{(\sqrt{n} + 2)} - 1]\gamma^{(\sqrt{n}-1)} - \alpha^{2\sqrt{n}}[\alpha^{(2-\sqrt{n})} - 1]\gamma^{-(n+1)}$$

$$- [\alpha^{2\sqrt{n}} - 1]\gamma \Bigg\} + \frac{(\nu_{\theta R} + 3)b}{(9 - n)[\alpha^{2\sqrt{n}} - 1]} \Bigg\{ [\alpha^{(\sqrt{n} + 3)} - 1]\gamma^{(\sqrt{n}-1)}$$

$$- \alpha^{2\sqrt{n}} [\alpha^{(3-\sqrt{n})} - 1]\gamma^{-(\sqrt{n} + 1)} - [\alpha^{2\sqrt{n}} - 1]\gamma \Bigg\} \tag{27}$$

and

$$\frac{\sigma_\theta}{jB_iR_i} = \frac{(\nu_{\theta R} + 2)(1 - b)\sqrt{n}}{(4 - n)[\alpha^{2\sqrt{n}} - 1]} \Bigg\{ [\alpha^{(\sqrt{n}+2)} - 1]\gamma^{(\sqrt{n} - 1)} + \alpha^{2\sqrt{n}}[\alpha^{(2-\sqrt{n})} - 1]\gamma^{-(\sqrt{n}+1)}$$

$$- [\alpha^{2\sqrt{n}} - 1] \frac{\sqrt{n}\,(1 + 2\nu_{R\theta})}{(\nu_{\theta r} + 2)} \gamma \Bigg\}$$

$$+ \frac{(\nu_{\theta R} + 3)b\sqrt{n}}{(9 - n)[\alpha^{2\sqrt{n}} - 1]} \Bigg\{ [\alpha^{(\sqrt{n} + 3)} - 1]\gamma^{(\sqrt{n} - 1)}$$

$$+ \alpha^{2\sqrt{n}}[\alpha^{(3 - \sqrt{n})} - 1]\gamma^{-(\sqrt{n} + 1)} - [\alpha^{2\sqrt{n}} - 1] \frac{\sqrt{n}(1 + 3\nu_{R\theta})}{(\nu_{\theta R} + 3)} \gamma^2 \Bigg\} \tag{28}$$

where

$$\nu_{R\theta} = \frac{\nu_{\theta R}}{n} .$$

H. Stress Equilibrium Check

A freebody diagram of a portion of a solenoid under the influence of electromechanical forces is shown in Fig. 2. The radial body force per unit volume, F_R, can be used to determine F_{VT}, the resultant vertical electromechanical force on this freebody. The integral of the hoop stress distribution over the area of the cut plane must equal the resultant force, or

$$F_{VT} = \int_{\text{cut area}} \sigma_\theta \, dA .$$

By changing variables F_{VT} may be expressed as

$$F_{VT} = 2R_i \ell_z \int_1^\alpha \sigma_\theta d\alpha \tag{29}$$

where ℓ_z is a significant dimension in the direction perpendicular to the plane of the cut. Substitution of Eq. (28) into the above equation and performance of the indicated operation yields

$$F_{VT} = 2\ell_z j B_i R_i^2 \left[\frac{b}{3} (\alpha^3 - 1) + \frac{(1 - b)}{2} (\alpha^2 - 1) \right] . \tag{30}$$

The resultant force can also be calculated by integrating the vertical component of F_R over the volume of the freebody:

$$F_{VT} = \int_{Vol} F_R \sin \theta dV.$$

If we substitute Eqs. (5) and (14) into the above expression and change the integrating variables, then

$$F_{VT} = jB_iR_i^2\ell_z \int_1^{\alpha} [1 + b\ (\gamma - 1)]\ \gamma d\gamma \int_o^{\pi} d\theta.$$

We then perform the integration:

$$F_{VT} = 2\ell_z jB_iR_i^2 \left[\frac{b}{3}(\alpha^3 - 1) + \frac{(1-b)}{2} (\alpha^2 - 1) \right].$$

Therefore, the hoop stress distribution in Eq. (28) does satisfy equilibrium and is a unique solution.

III. RESULTANT ELECTROMECHANICAL DISPLACEMENT, STRESSES, AND STRAINS IN AN AXISYMMETRIC TRANSVERSELY ISOTROPIC SOLENOID

The effect of transverse isotropy on the displacement, stresses, and strains in a solenoid under the influence of electromechanical forces is demonstrated with the following three examples. All three examples assume boundary conditions, magnetic fields, and current approximations consistent with the assumptions presented in the previous section. For consistency the magnetic field at the inner and outer radius for all three examples is calculated by assuming β, the ratio of the magnet height to inner diameter, to be twice α and by assuming j to be constant. These two assumptions produce a radially varying, axial magnetic field which approximates a straight line at the magnet midplane in each example. (The error involved is discussed in Sec. IV.)

The ratios of outer to inner radius, α, for the three examples are 1.2, 2.0, and 16.0. These geometries illustrate an interesting range of behavior in the displacement, stress, and strain distributions in a solenoid. Within this range the radial stress distribution changes from being negative throughout the magnet ($\alpha = 1.2$) to being almost entirely positive ($\alpha = 16.0$); the location of maximum deflection moves into the magnet for increasing α; and, significantly, the maximum hoop stress actually decreases for $\alpha > 2.0$ and increasing transverse isotropy.

In all three examples the material constants E_θ and $\nu_{\theta R}$ are the same with $\nu_{\theta R} = 0.33$. Each graph presents a nondimensional parameter as a function of γ, the normalized radius, for four values of n ranging from 1.0 to 10.0. This range was chosen to reflect a reasonable range of magnet material behavior from isotropic (n = 1.0) to highly transversely isotropic (n = 10.0).

The significant parameters presented graphically for each example are:

(1) the nondimensional displacement, u^*,

$$u^* = \frac{uE_\theta}{jB_1R_1^2} \quad ;$$

(2) the nondimensional stresses, σ_R^* and σ_θ^*,

$$\sigma_R^* = \frac{\sigma_R}{\xi} = \frac{\sigma_R}{jB_iR_i}$$

and

$$\sigma_\theta^* = \frac{\sigma_\theta}{\xi} = \frac{\sigma_\theta}{jB_iR_i} \ ;$$

(3) the normalized strains, ε_R^* and ε_θ^* ,

$$\varepsilon_R^* = \frac{\varepsilon_R E_\theta}{jB_iR_i}$$

and

$$\varepsilon_\theta^* = \frac{\varepsilon_\theta E_\theta}{jB_iR_i} \ .$$

A. Displacement, Stresses, and Strains for $\alpha = 1.2$

The nondimensional radial displacement plotted against γ (the nondimensional radius) is shown in Fig. 3 for a solenoid of a geometry $\alpha = 1.2$ and $\beta = 1.4$. As would be expected, the maximum displacement increases with increasing transverse isotropy, since this has the effect of locally decreasing the magnet stiffness. (E_θ is constant.)

The distribution of the nondimensional radial and hoop stresses vs γ is presented in Figs. 4 and 5. For this solenoid, increasing transverse isotropy slightly decreases the magnitude of the radial stress distribution which is compressive or negative throughout the magnet and correspondingly slightly increases the maximum hoop stress.

The normalized radial and hoop strain distribution is plotted vs γ in Figs. 6 and 7. As the radial stiffness decreases for increasing transverse isotropy, the radial deflection and strain must increase.

B. Displacement, Stresses, and Strains for $\alpha = 2.0$

The following example, which is presented because it demonstrates the beginning of a change in the character of the solution, pertains to a solenoid of geometry $\alpha = 2.0$ and $\beta = 4.0$. The graphs of nondimensional displacement, nondimensional stresses, and the normalized strains are shown in Figs. 8 through 12. All except the radial stress generally exhibit the same characteristics that were illustrated in the previous example. However, the radial stress distribution is positive for a small range of γ.

This is significant since now there is a mechanism which tends to force gaps to develop within the magnet. If gaps can develop, such as in an unpotted layer-wound magnet, care must be used when calculating a solution of this type to ensure that sufficient mechanical preload has been applied to the windings.

C. Displacements, Stresses, and Strains for $\alpha = 16.0$

Figure 13 illustrates the nondimensional displacement vs γ for a solenoid with dimensions of $\alpha = 16.0$ and $\beta = 32.0$. This graph clearly presents the effect of transverse isotropy upon the character of the displacement within the magnet. As the transverse isotropy increases, the radial stiffness decreases and, therefore, the average displacement must increase.

The nondimensional radial stress vs γ is plotted in Fig. 14. As the transverse isotropy increases (n increases), the magnet tends to act like a collection of independent hoops which cannot transmit radial force, thus causing the radial stress to approach zero.

The nondimensional hoop stress vs γ is presented in Fig. 15, which illustrates a very significant result; for thick solenoids, as the transverse isotropy increases, the peak hoop stress not only decreases in magnitude, but also occurs at a location other than the inner radius. This phenomenon can be explained by again using the radially unsupported hoop analogy. Examination of the radial body force distribution within the magnets yields

$$F_R = \frac{df_R}{dV} = jB_i \, [1 + b(\gamma - 1)]$$

where f_R is the body force. Rearranging and nondimensionalizing yield

$$\frac{df_R^*}{d\gamma} = \frac{df_R}{d\gamma}\left[\frac{1}{jB_iR_i^2\ell_z}\right] = 2\pi \, [1 + b(\gamma - 1)]\gamma \quad . \tag{31}$$

A plot of the derivative of the nondimensional body force with respect to γ vs γ is shown in Fig. 16 for several geometries, including the three presented in this section. The manner in which the body force changes with respect to radial position is fundamental in understanding the difference between the behavior of the example solenoids.

For a thin magnet the body force is greatest at the inner surface and decreases throughout the magnet. In fact, if B_o is approximately zero, then it can be shown that for $\alpha \leq 2.0$, the maximum force is on the inner surface.

For $\alpha > 2.0$ the maximum force for $B_o = 0$ is at the location $R_o/2.0$, which is within the windings of the magnet. Remembering the hoop analogy — that each hoop does not transmit radial force and must support itself — then the hoop stress should be the image of the shape of the body force change for a highly transversely isotropic case. This is in contrast to the isotropic case where there is a radial transmission of load which forces the peak stress to occur at the inner surface.

For completeness the normalized radial and hoop strains for $\alpha = 16.0$ are presented in Figs. 17 and 18.

IV. ELECTROMAGNETIC CONSIDERATIONS

The purpose of this section is to estimate the error involved in using a linear magnetic field variation in the solenoid windings, and so to present a set of normalized field factors to aid in evaluating B_i and B_o as input to the formulation in previous sections.

The normalized field factors calculated are unit dependent and are presented to reflect MKS units.

A. Effect of Linear Field Variation

The analysis in Sec. 2 assumes a linear variation in the axial component of magnetic field through the solenoid windings. This approximation is known to be very good for long, thin solenoids where the field in the windings can be treated like the field in an infinite current slab with finite thickness. It is not clear, however, how good this approximation is for other rectangular winding shapes. Since the central issue for this report is the stress in the windings due to the electromagnetic forces, the basis for comparison will be the integrated radial force per unit axial length in the midplane of the solenoid. The integrated (or total) radial force is given by

$$F = 2\pi j \int_{R_i}^{R_o} B_z R dR \quad . \tag{32}$$

The total force for the linear approximation will be designated as F_ℓ and the total force for the true field shape will be designated as F_m. F_ℓ is computed by calculating B_i and B_o with a solenoid field code and then integrating Eq. (32) with the field as a linear function of radius. F_m is calculated by numerically integrating Eq. (32) with the actual variation of the field. The percent error, E, in F_ℓ is

$$E = \frac{F_\ell - F_m}{F_m} 100. \tag{33}$$

Since the field variation is a function of α and β, then F_ℓ, F_m, and E are also functions of α and β. Figure 19 is a contour plot of constant values of E over the range $1 < \alpha \leq 5$, $0.1 \leq \beta \leq 5$; it shows that for some cases the linear field variation overestimates the total radial force and for some cases underestimates it. The relative density of contour levels for $E > 0$ and $E < 0$ shows that the magnitude of E changes more rapidly in the region of $E < 0$ than in the $E > 0$ region. Figure 20 is a contour plot of constant values of E over extended ranges of α and β. Although the α-axis range is from 0 to 16, the smallest physically possible α is 1.0. On this contour, the largest error for $E > 0$ is 7.6%; the largest error for $E < 0$ is about 20%. The region of largest error is for $\beta < 1$ and $\alpha > 2$; therefore, care should be taken when analyzing isolated pancake coils. However, for a majority of solenoidal geometries, the linear field approximation yields acceptable results.

B. Normalized Field Factors

The concept of normalized field factors is well known and is often used to give quick field value estimates in the early stages of magnet design. Two sets of normalized field factors are needed to estimate B_i and B_o. B_i is given by the expression

$$B_i = B_i^* R_i j \tag{34}$$

and B_o is given by

$$B_o = B_o^* R_i j \tag{35}$$

where R_i has units of meters, j has units of amperes per square meter, and B_o and B_i have units of tesla. B_i^* and B_o^* are functions of α and β and are calculated by Eqs. (34) and (35) using a solenoid field code. Contours of constant values of B_i^* are presented in Fig. 21 and for an extended range in Fig. 22. Contours of constant values of B_o^* are presented in Fig. 23 and for an extended range in Fig. 24. These contour plots may be used to determine B_i^* and B_o^* graphically given the α and β of a solenoid. Performing the multiplication in Eqs. (34) and (35) using R_i in meters and j in amperes per square meter, yields the inner and outer magnetic fields in tesla.

V. MAXIMUM ELECTROMECHANICAL STRESS CONTOUR PLOTS

By extending the field factor concept to the computation of stresses, contours of constant values of maximum hoop stress can be calculated using Eq. (28). The maximum hoop stress is normalized by the expression

$$\sigma_{max} = \sigma_\theta^* B_i R_i j \tag{36}$$

where σ_{max} has units of pascals (N/m^2), B_i has units of tesla, R_i has units of meters, j has units of amperes per square meter, and σ_θ^* is read from the following contour plots.

The following contour plots represent the normalized hoop stress factor, σ_θ^*, for various rectangular solenoid geometries. For this single material, radially unsupported approximation, the hoop stress depends upon the ratio of the hoop to radial elastic modulus, n; therefore four graphs are presented for four different values of n. Figures 25, 26, 27, and 28 represent the hoop stress factor for n equal to 1.0, 2.0, 5.0, and 10.0, respectively.

VI. CONCLUSIONS

A solution for the displacement, stress, and strain in a transversely isotropic, axisymmetric, electromechanically loaded solenoid has been derived. The solution has the characteristic that for thick solenoids ($\alpha > 2.0$) the maximum hoop stress may occur in the interior of the coil windings, if the transverse isotropy is high.

This paper also graphically presents several design aids in the form of field factors and maximum hoop stress factors.

The maximum hoop stress factors cover the range from isotropic to highly transversely isotropic material behavior. From these factors a rapid estimate may be obtained of the maximum electromechanical hoop stress developed within a solenoid.

REFERENCES

1. L. M. Lontai and P. G. Marston, "A 100 Kilogauss Quasi-Continuous Cryogenic Solenoid — Part I," Proc. Intl. Symposium on Magnet Technology, ed. by H. Brechna and H. S. Gordon (1965).

2. W. F. Westendorp and R. W. Kilb, "Stresses in Magnetic Field Coils," p. 714 in Proc. 1968 Summer Study on Superconducting Devices and Accelerators, Part III, BNL 50155 (C-55), Brookhaven National Laboratory, Upton, Long Island, New York (April 1969).

3. H. Burkhard, J. Phys. D 6, 357 (1975).

4. A. A. Kuznetsov, Zh. Tekh. Phys. 30(5), 589 (1960) [Sov. Phys.-Tech. Phys. 5(5), 552 (1960)].

5. B. Léon, Revue Generale de l'Electricité 73(12), 632 (1964)(translated by W. G. Stripp).

6. N. E. Johnson, "The Stress Analysis of Non-Homogeneous Superconducting Solenoids," paper presented at the 1975 Cryogenics Materials Conference, Kingston, Ontario, Canada, July 22-25, 1975.

7. N. E. Johnson, The Structural Analysis of Non-Homogeneous Solenoids Using the STANSOL Computer Program, MRI-C2754-TR-3, Mechanics Research, Inc., Oak Ridge, Tennessee (September 1975).

8. N. E. Johnson, W. H. Gray, and R. A. Weed, "Stress Analysis of Non-Homogeneous, Transversely Isotropic Superconducting Solenoids," Proc. 6th Symposium on Engineering Problems of Fusion Research (1976).

9. V. G. Novitskii and V. N. Shakhtarin, "Electro-Dynamic Strains and Mechanical Stresses in Superconducting Magnetic Systems," translated from the Russian (Dokl. Akad. Nauk SSSR, Energetika i

Transport, No. 2, pp. 50-55, 1972) and published as ORNL-tr-2902, Oak Ridge National Laboratory, Oak Ridge Tennessee (1972).

10. W. H. Gray and C. T. Sun, Theoretical and Experimental Determination of Mechanical Properties of Superconducting Wire, ORNL/TM-5331, Oak Ridge National Laboratory, Oak Ridge, Tennessee (July 1976).

11. J. E. Ashton and J. C. Halpin, Primer on Composite Materials: Analysis (Tecknomic Publishing Co., Inc., Stanford, Connecticut, 1969).

12. The Poisson ratio between the radial and hoop direction is also referred to as the major Poisson ratio.

13. Another application of rotational transverse isotropy can be found when the mechanical properties of tree trunks are examined.

14. E. Kreyszig, Advanced Engineering Mathematics (John Wiley and Sons, New York, 1967), 2nd ed., p. 116.

FIGURE CAPTIONS

Fig. 1. Solenoid coordinate system.

Fig. 2. Solenoid freebody diagram.

Fig. 3. Nondimensional deflection vs nondimensional position for four values of transverse isotropy and $\alpha = 1.2$.

Fig. 4. Nondimensional radial stress vs nondimensional position for four values of transverse isotropy and $\alpha = 1.2$.

Fig. 5. Nondimensional hoop stress vs nondimensional position for four values of transverse isotropy and $\alpha = 1.2$.

Fig. 6. Nondimensional radial strain vs nondimensional position for four values of transverse isotropy and $\alpha = 1.2$.

Fig. 7. Nondimensional hoop strain vs nondimensional position for four values of transverse isotropy and $\alpha = 1.2$.

Fig. 8. Nondimensional deflection vs nondimensional position for four values of transverse isotropy and $\alpha = 2.0$.

Fig. 9. Nondimensional radial stress vs nondimensional position for four values of transverse isotropy and $\alpha = 2.0$.

Fig. 10. Nondimensional hoop stress vs nondimensional position for four values of transverse isotropy and α = 2.0.

Fig. 11. Nondimensional radial strain vs nondimensional position for four values of transverse isotropy and α = 2.0.

Fig. 12. Nondimensional hoop strain vs nondimensional position for four values of transverse isotropy and α = 2.0.

Fig. 13. Nondimensional deflection vs nondimensional position for four values of transverse isotropy and α = 16.0.

Fig. 14. Nondimensional radial stress vs nondimensional position for four values of transverse isotropy and α = 16.0.

Fig. 15. Nondimensional hoop stress vs nondimensional position for four values of transverse isotropy and α = 16.0.

Fig. 16. Change of the normalized body force distribution with respect to position vs nondimensional position for five geometrically different solenoids.

Fig. 17. Nondimensional radial strain vs nondimensional position for four values of transverse isotropy and α = 16.0.

Fig. 18. Nondimensional hoop strain vs nondimensional position for four values of transverse isotropy and α = 16.0.

Fig. 19. A contour plot of constant values of the error between F_ℓ and F_m in percent vs α and β for the range $1 \leq \alpha \leq 5$ and $0.1 \leq \beta \leq 5$.

Fig. 20. A contour plot of constant values of the error between F_ℓ and F_m in percent vs α and β for the range $1 \leq \alpha \leq 16$ and $0.1 \leq \beta \leq 20$.

Fig. 21. A contour plot of constant values of the normalized field factor at the inside solenoid radius vs α and β for the range $1 \leq \alpha \leq 5$ and $0.1 \leq \beta \leq 5$.

Fig. 22. A contour plot of constant values of the normalized field factor at the inside solenoid radius vs α and β for the range $1 \leq \alpha \leq 16$ and $0.1 \leq \beta \leq 20$.

Fig. 23. A contour plot of constant values of the normalized field factor at the outside solenoid radius vs α and β for the range $1 \leq \alpha \leq 5$ and $0.1 \leq \beta \leq 5$.

Fig. 24. A contour plot of constant values of the normalized field factor at the outside solenoid radius vs α and β for the range $1 \leq \alpha \leq 16$ and $0.1 \leq \beta \leq 20$.

Fig. 25. A contour plot of constant values of the normalized electromechanical hoop stress vs α and β for $n = 1.0$.

Fig. 26. A contour plot of constant values of the normalized electromechanical hoop stress vs α and β for $n = 2.0$.

Fig. 27. A contour plot of constant values of the normalized electromechanical hoop stress vs α and β for $n = 5.0$.

Fig. 28. A contour plot of constant values of the normalized electromechanical hoop stress vs α and β for $n = 10.0$.

ORNL-DWG 76-18117

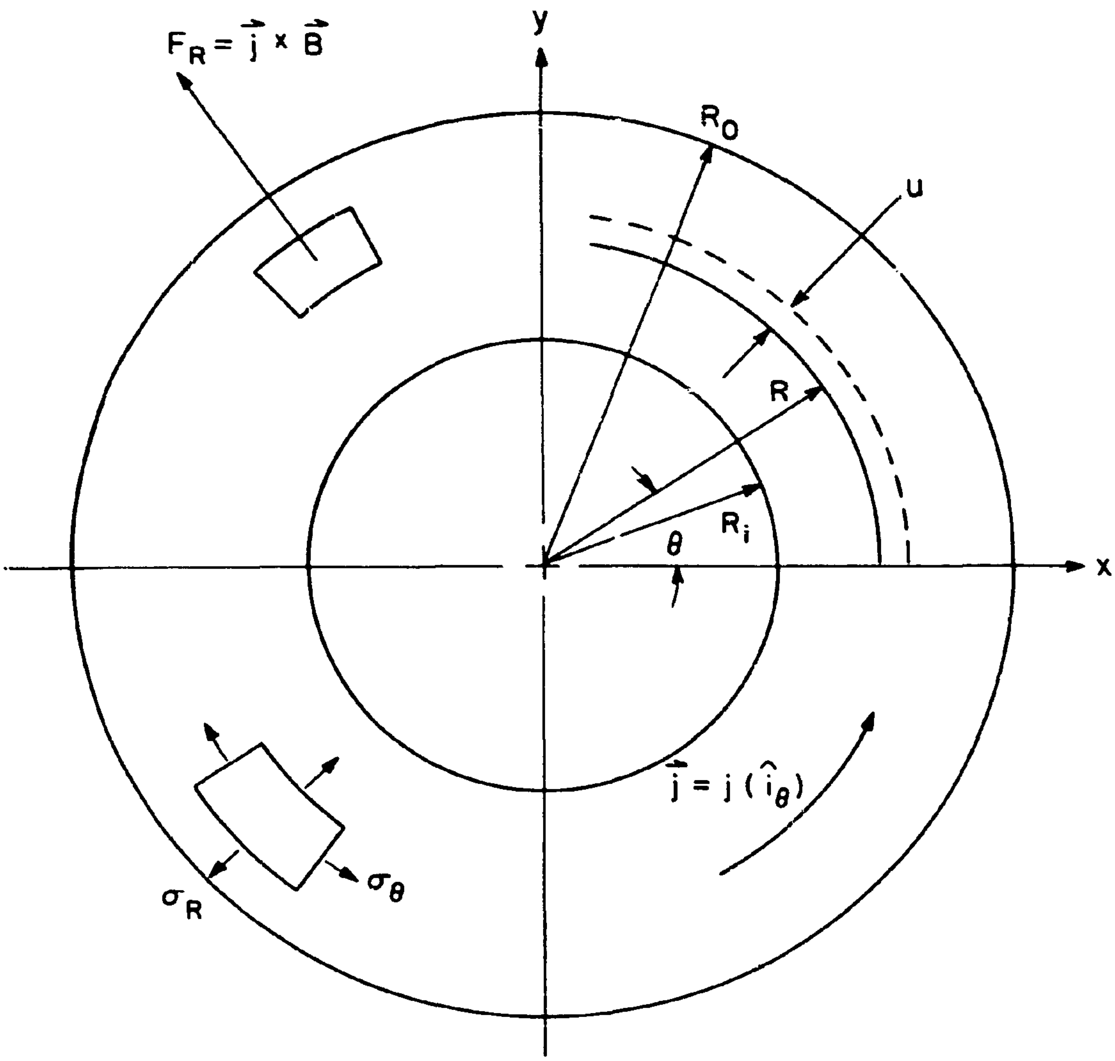

Fig. 1. Solenoid coordinate system.

ORNL-DWG 76-18118

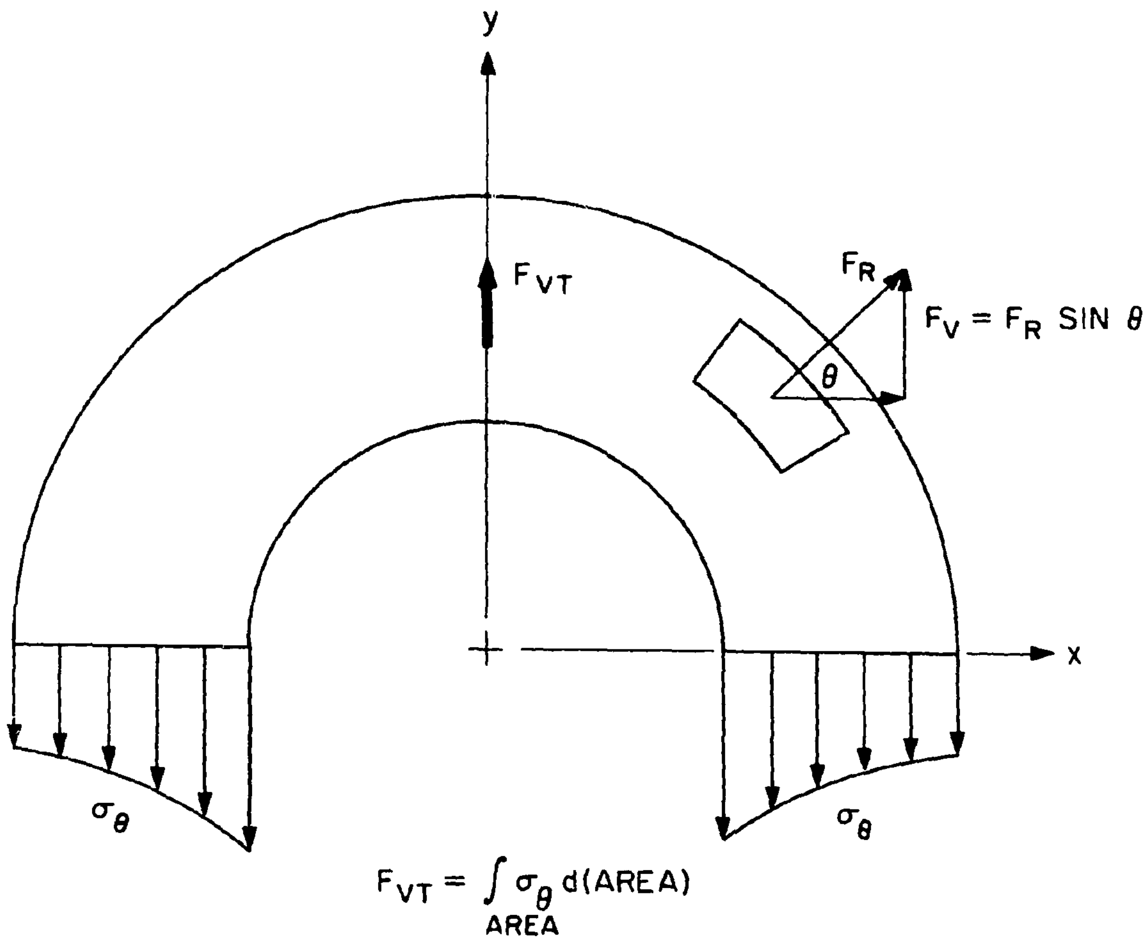

Fig. 2. Solenoid freebody diagram.

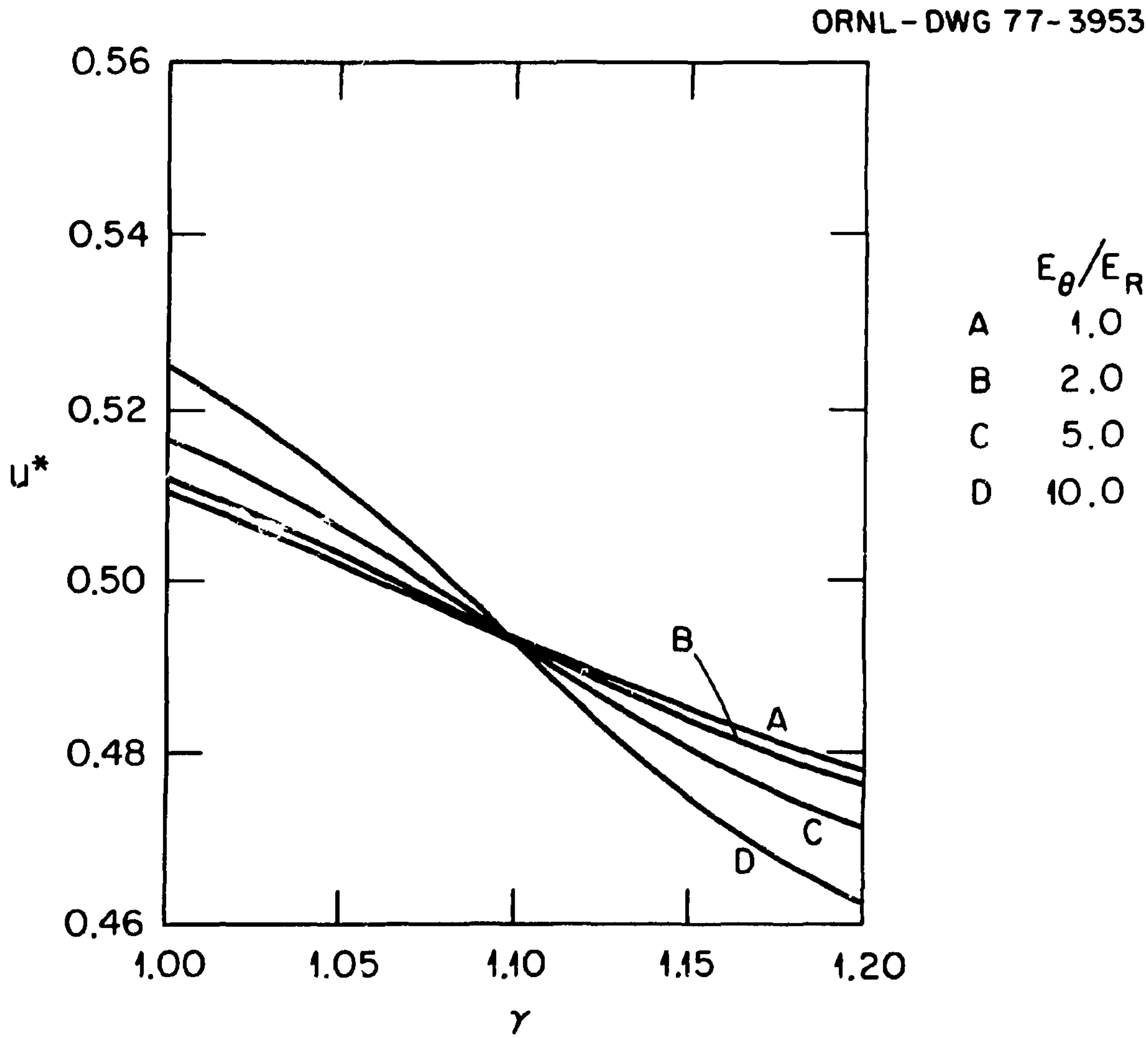

Fig. 3. Nondimensional deflection vs nondimensional position for four values of transverse isotropy and α = 1.2.

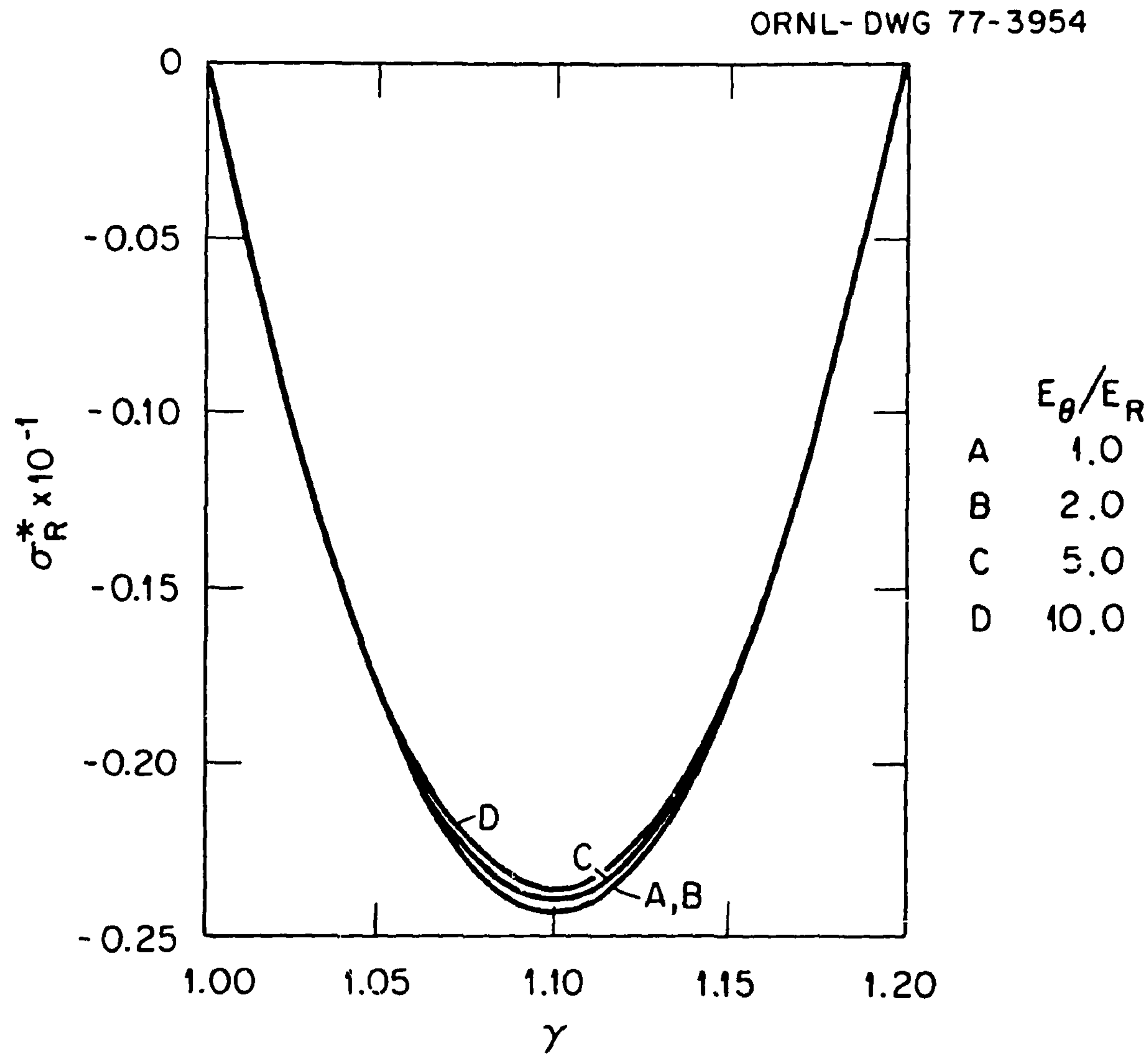

Fig. 4. Nondimensional radial stress vs nondimensional position for four values of transverse isotropy and α = 1.2.

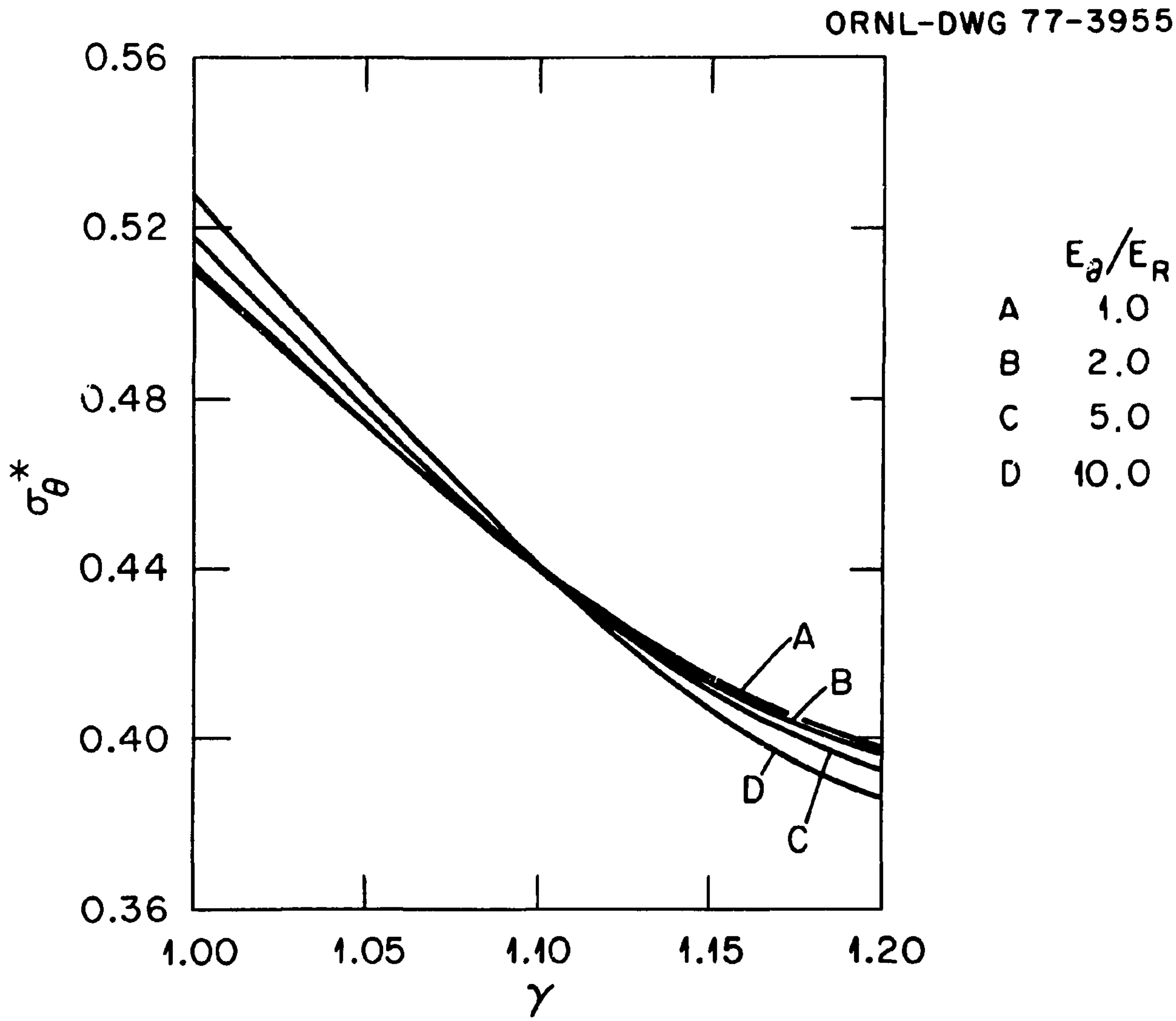

Fig. 5. Nondimensional hoop stress vs nondimensional position for four values of transverse isotropy and $\alpha = 1.2$.

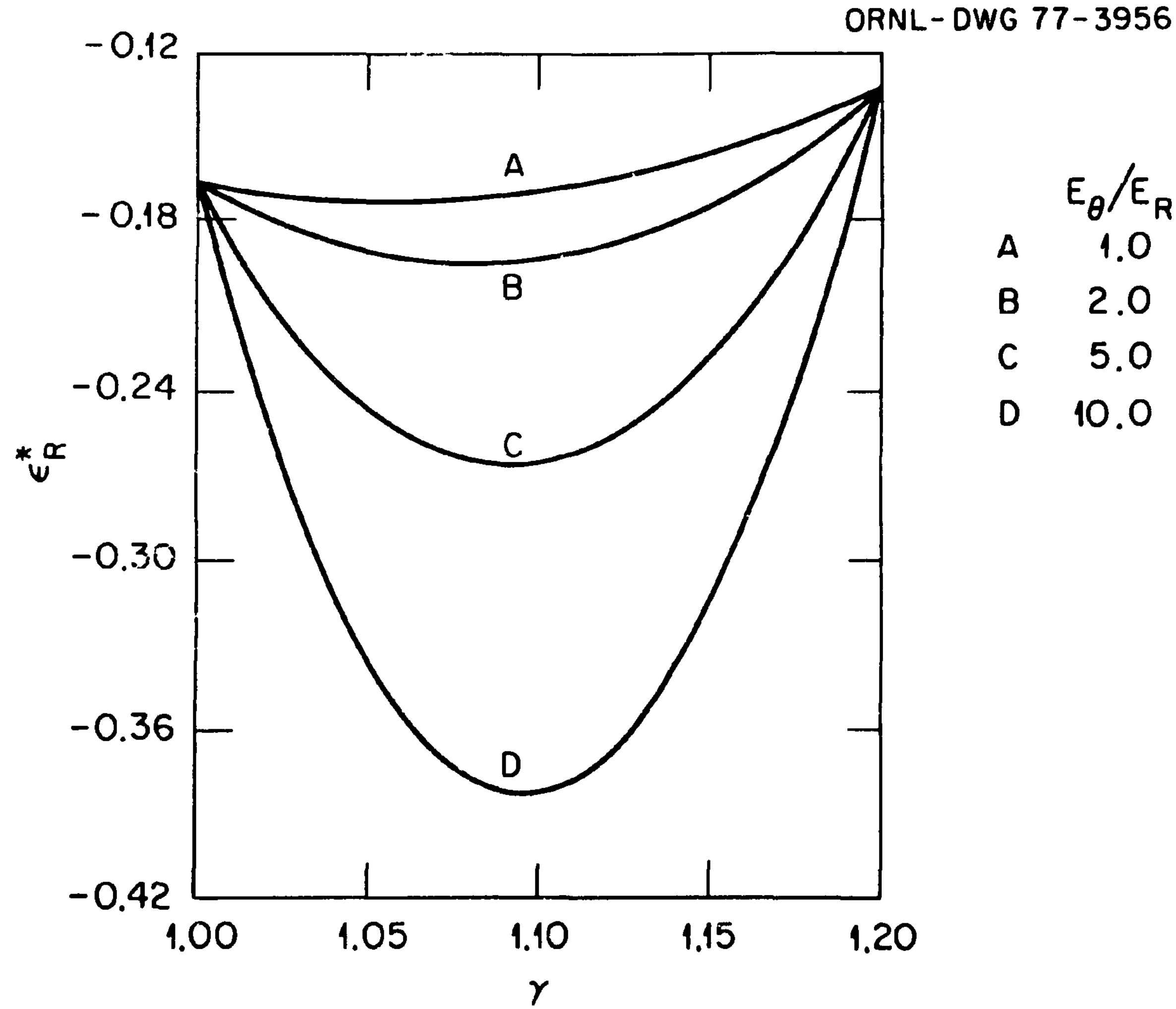

Fig. 6. Nondimensional radial strain vs nondimensional position for four values of transverse isotropy and α = 1.2.

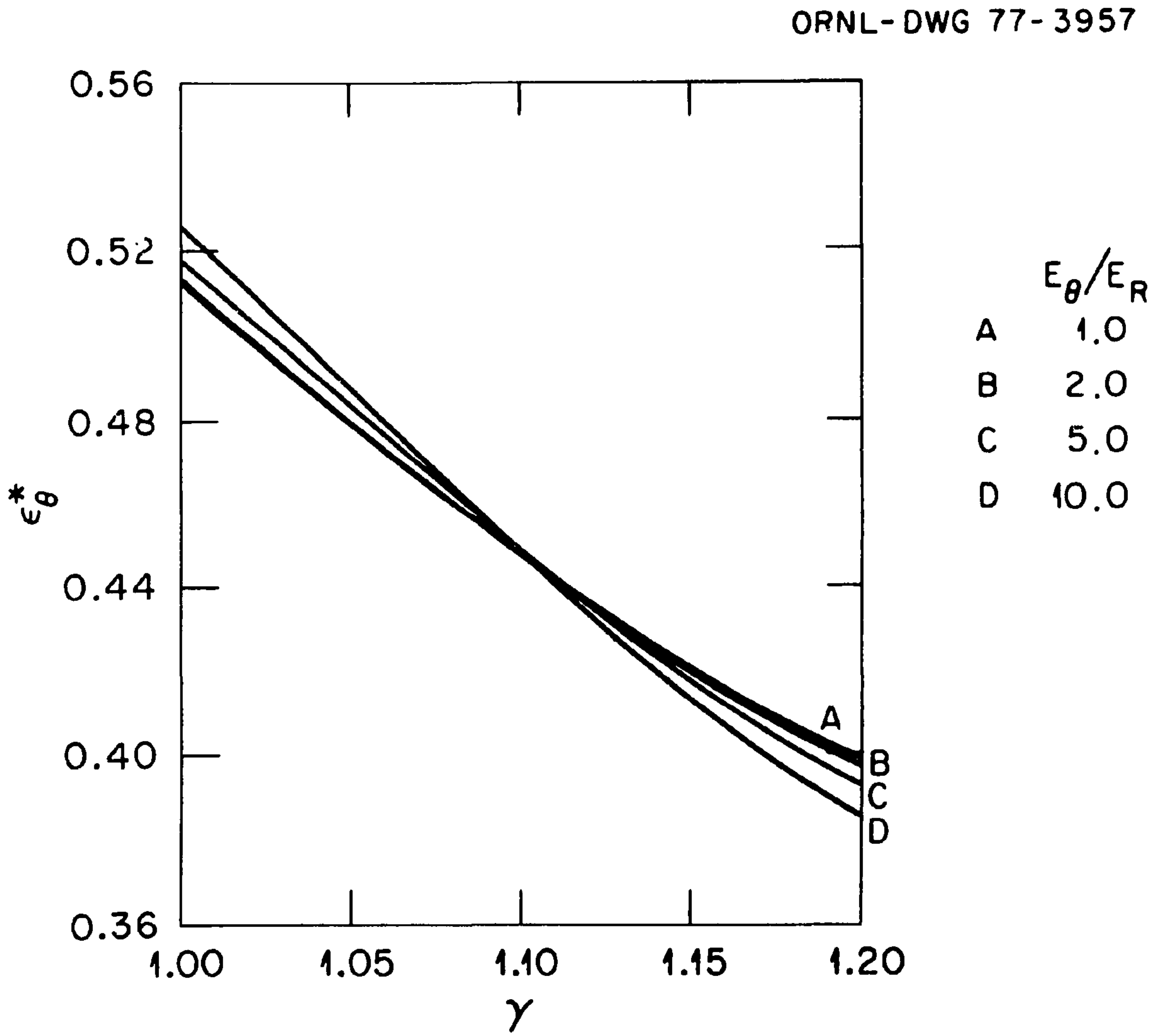

Fig. 7. Nondimensional hoop strain vs nondimensional position for four values of transverse isotropy and $\alpha = 1.2$.

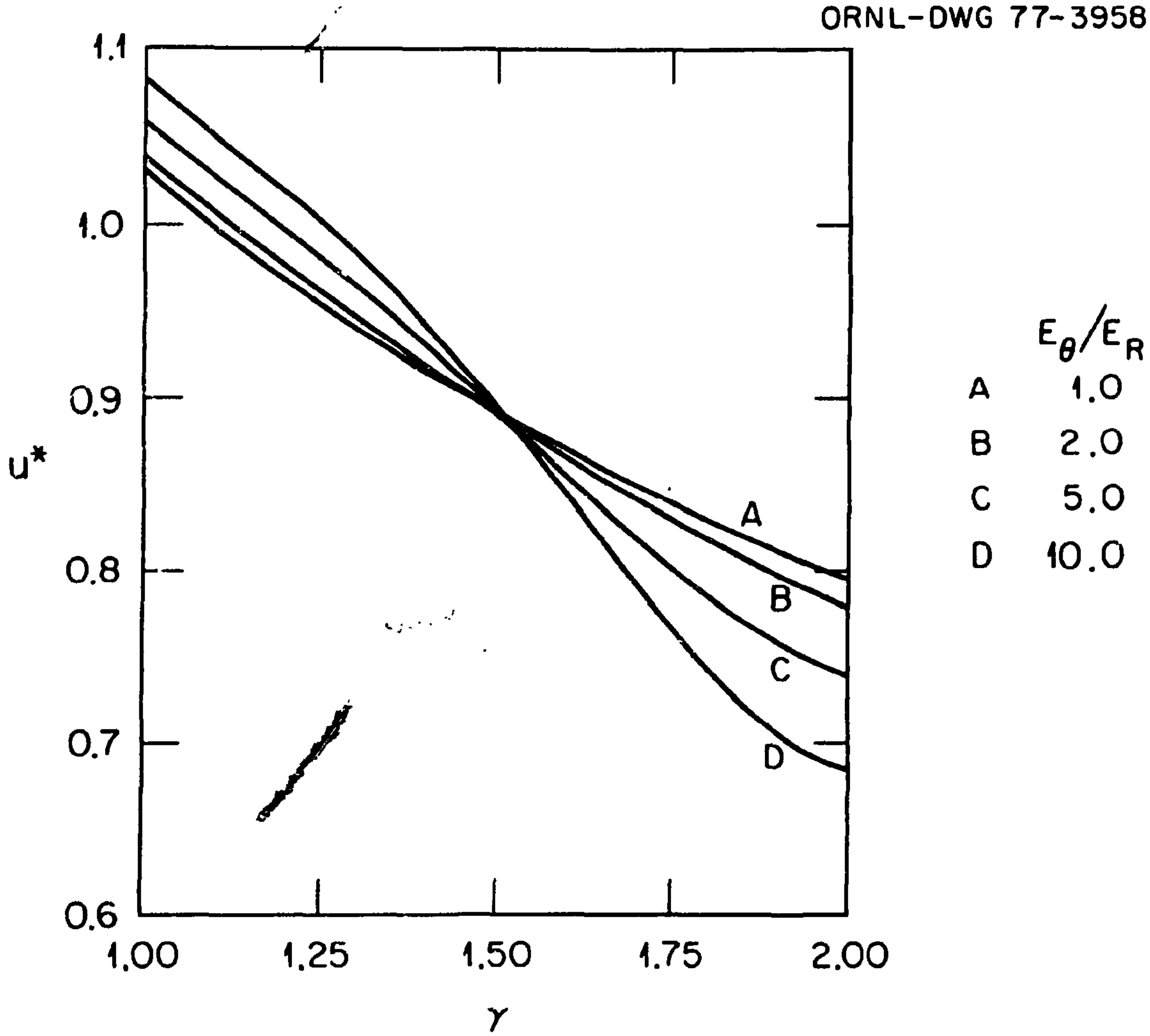

Fig. 8. Nondimensional deflection vs nondimensional position for four values of transverse isotropy and $\alpha = 2.0$.

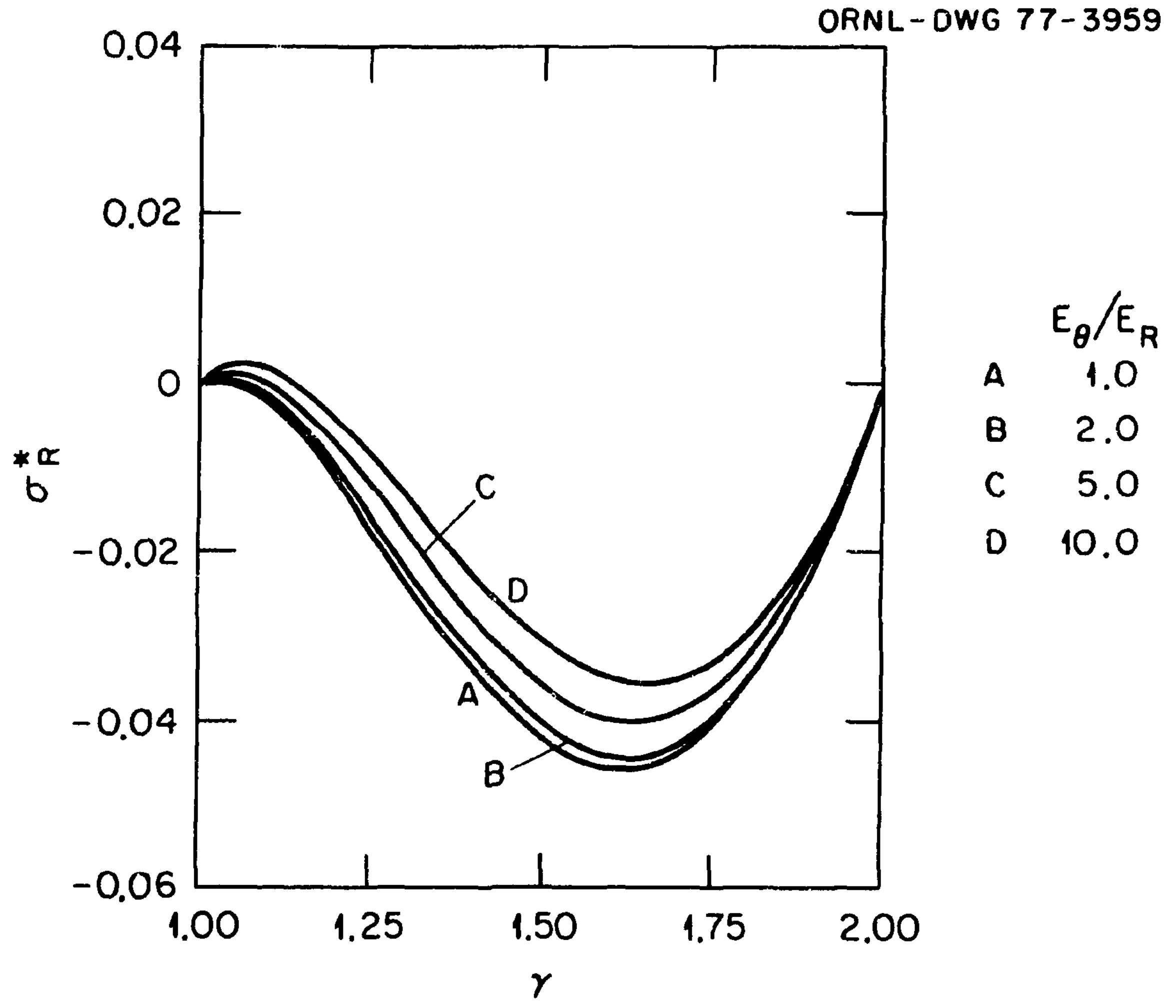

Fig. 9. Nondimensional radial stress vs nondimensional position for four values of transverse isotropy and α = 2.0.

ORNL-DWG 77-3960

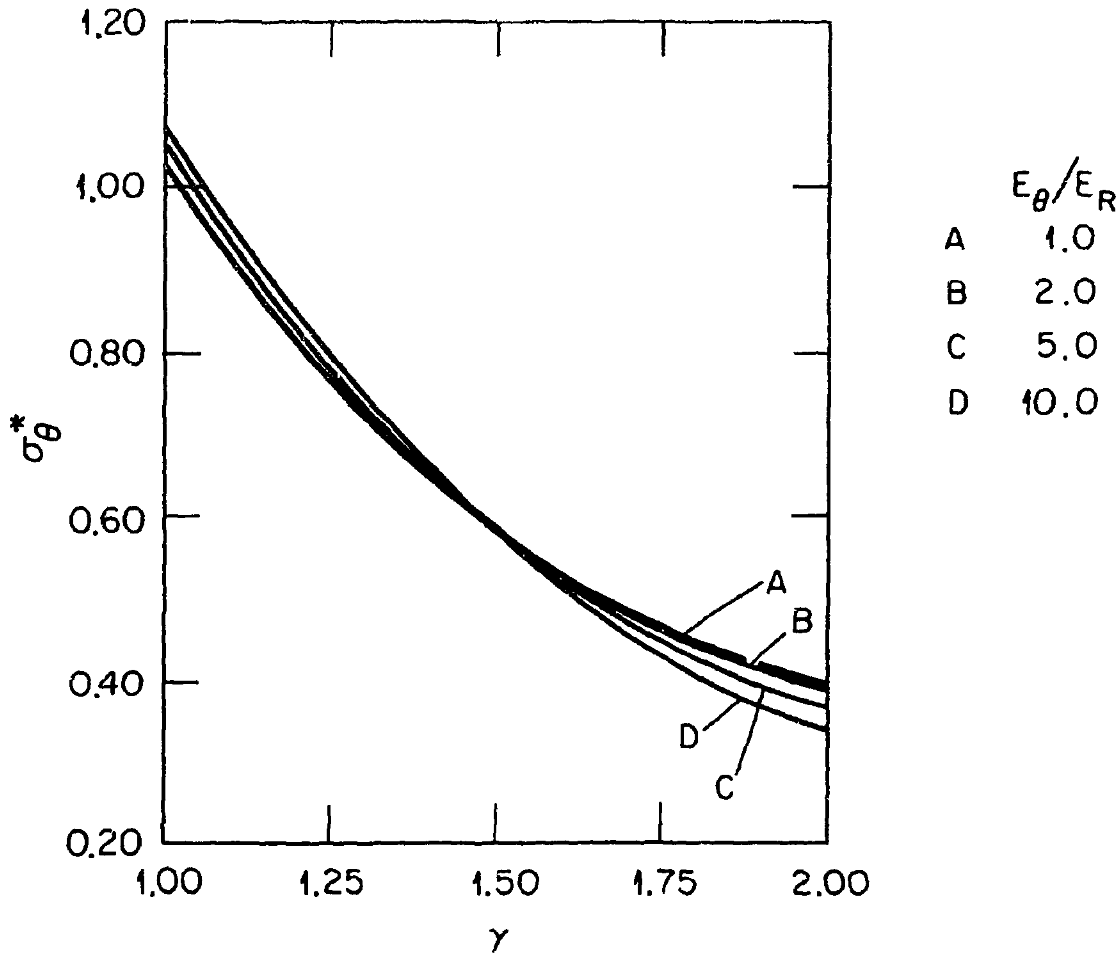

Fig. 10. Nondimensional hoop stress vs nondimensional position for four values of transverse isotropy and α = 2.0.

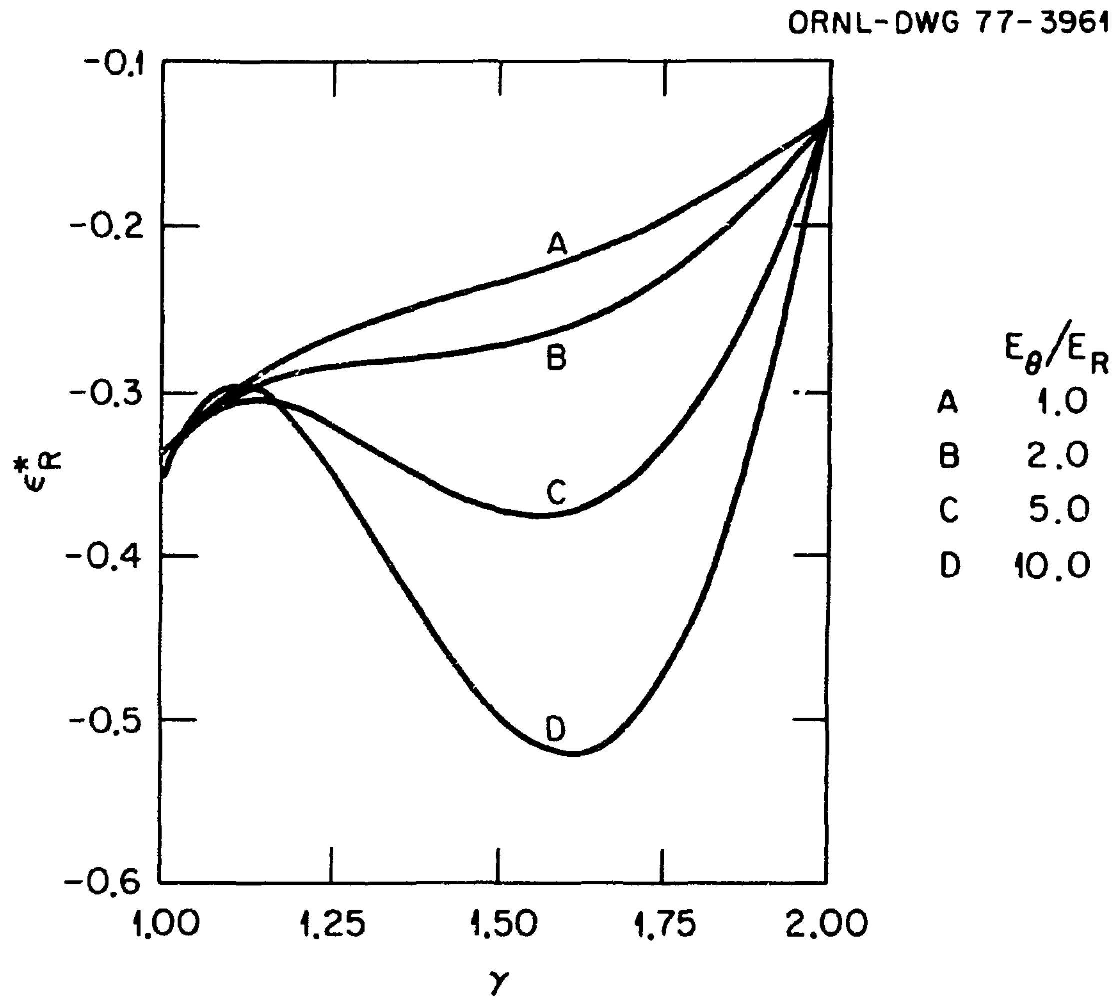

Fig. 11. Nondimensional radial strain vs nondimensional position for four values of transverse isotropy and α = 2.0.

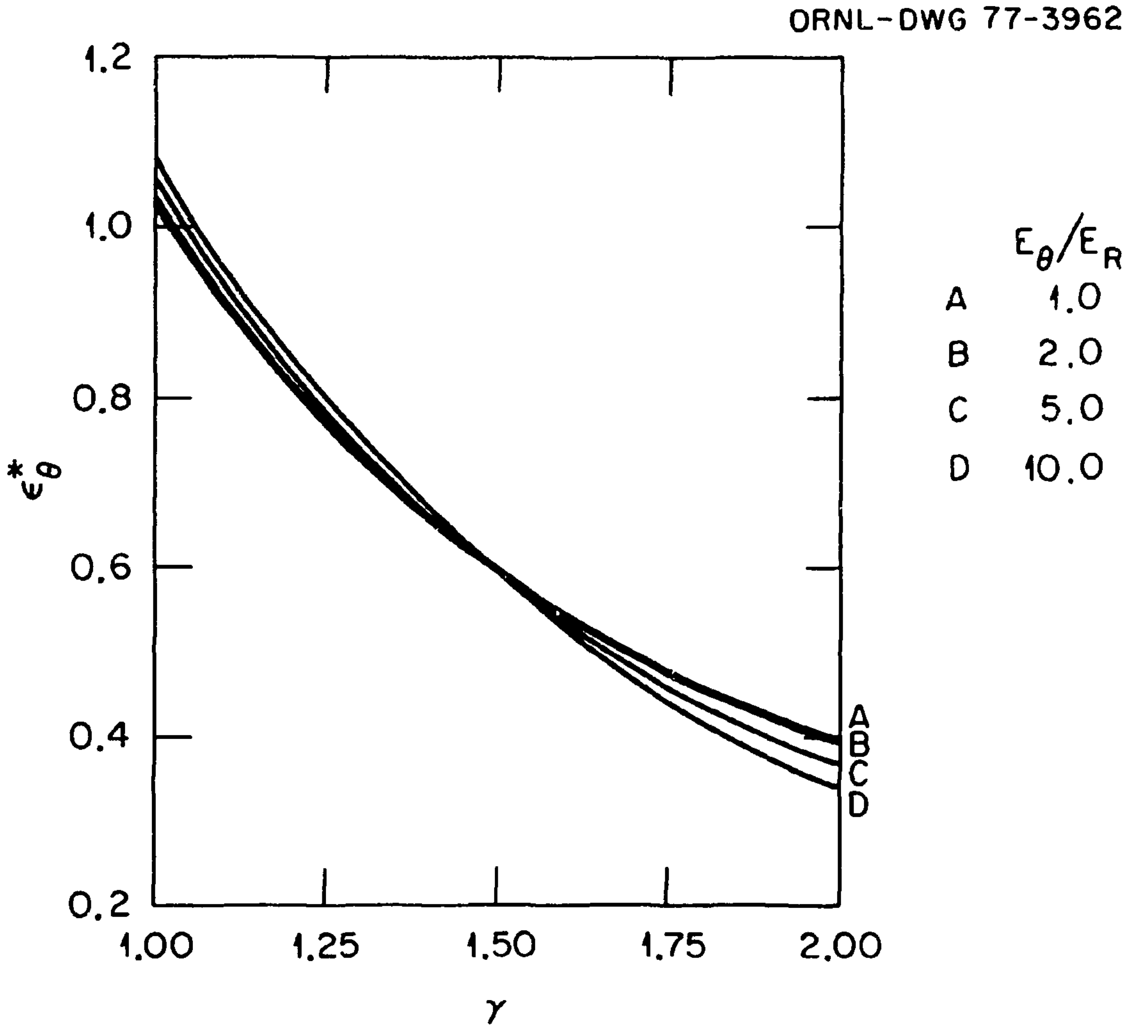

Fig. 12. Nondimensional hoop strain vs nondimensional position for four values of transverse isotropy and α = 2.0.

ORNL-DWG 77-3963

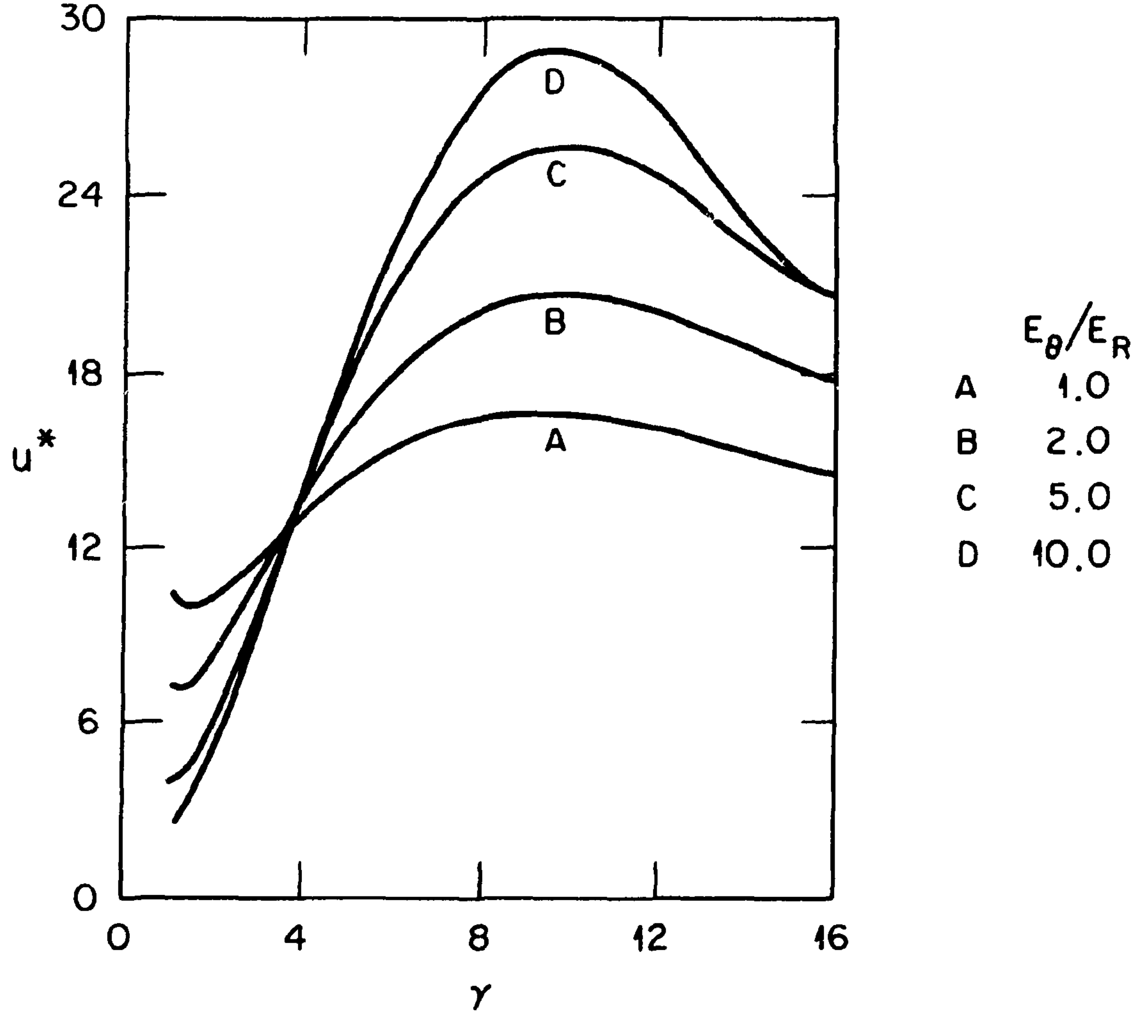

Fig. 13. Nondimensional deflection vs nondimensional position for four values of transverse isotropy and α = 16.0.

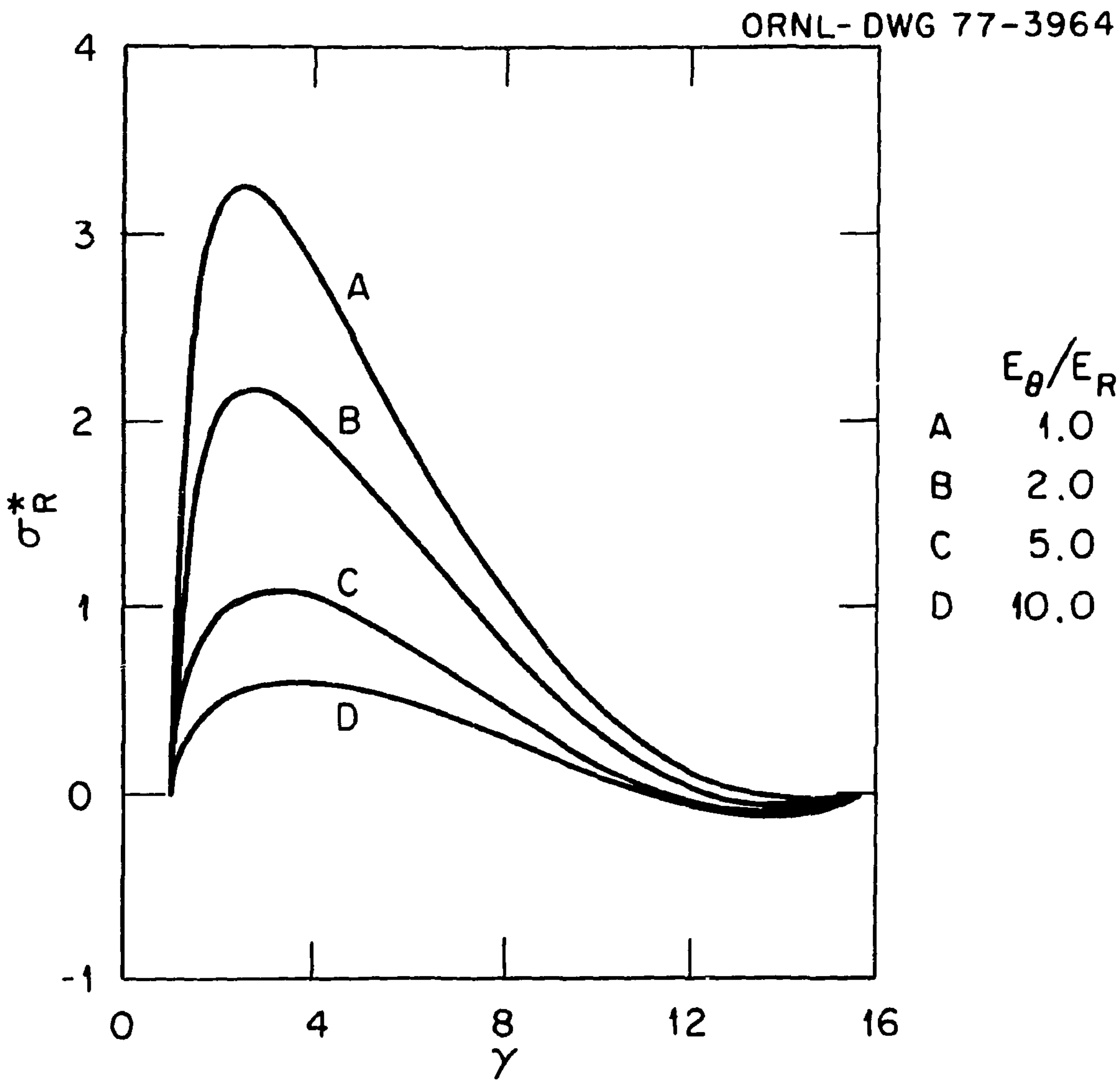

Fig. 14. Nondimensional radial stress vs nondimensional position for four values of transverse isotropy and α = 16.0.

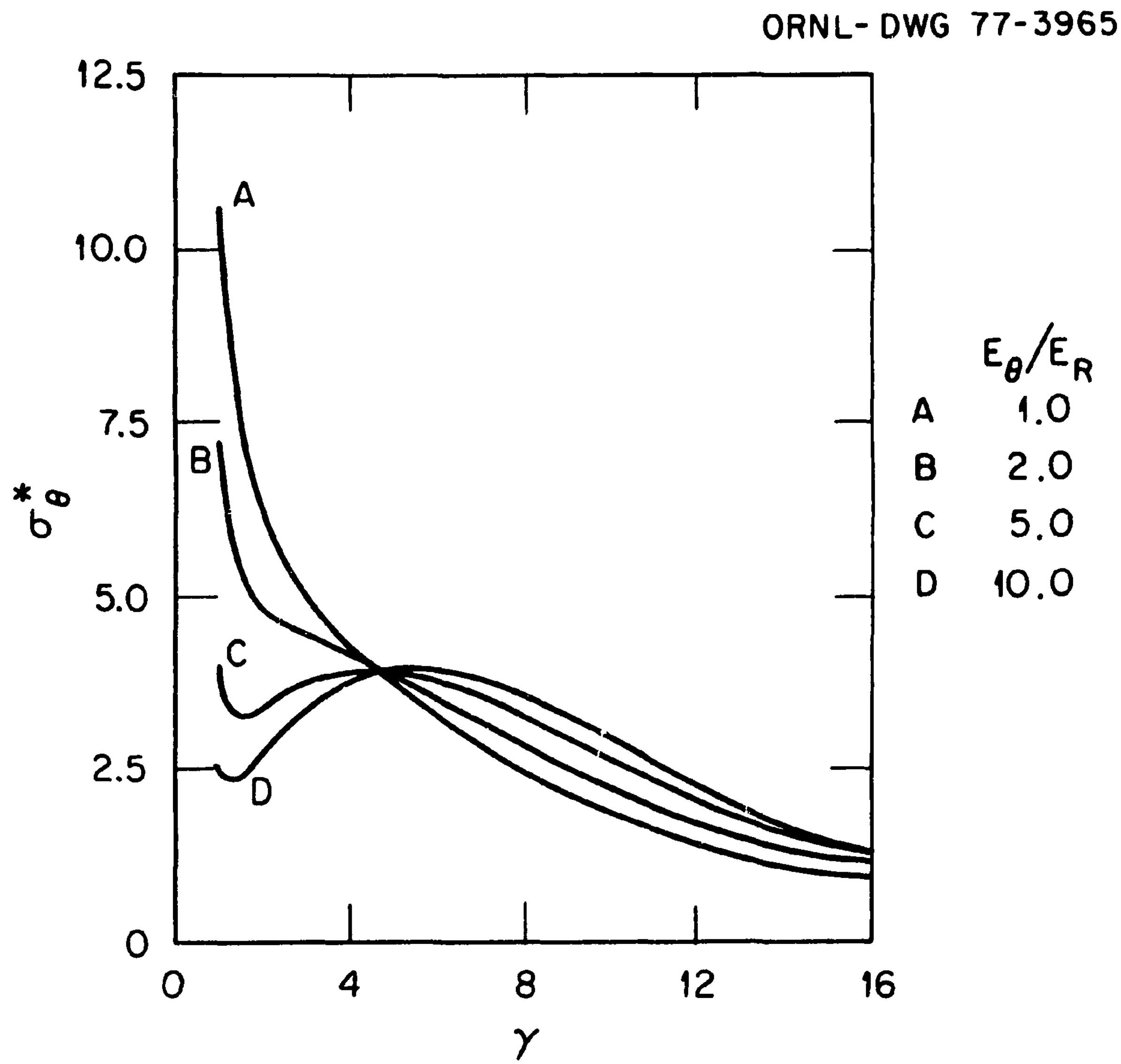

Fig. 15. Nondimensional hoop stress vs nondimensional position for four values of transverse isotropy and $\alpha = 16.0$.

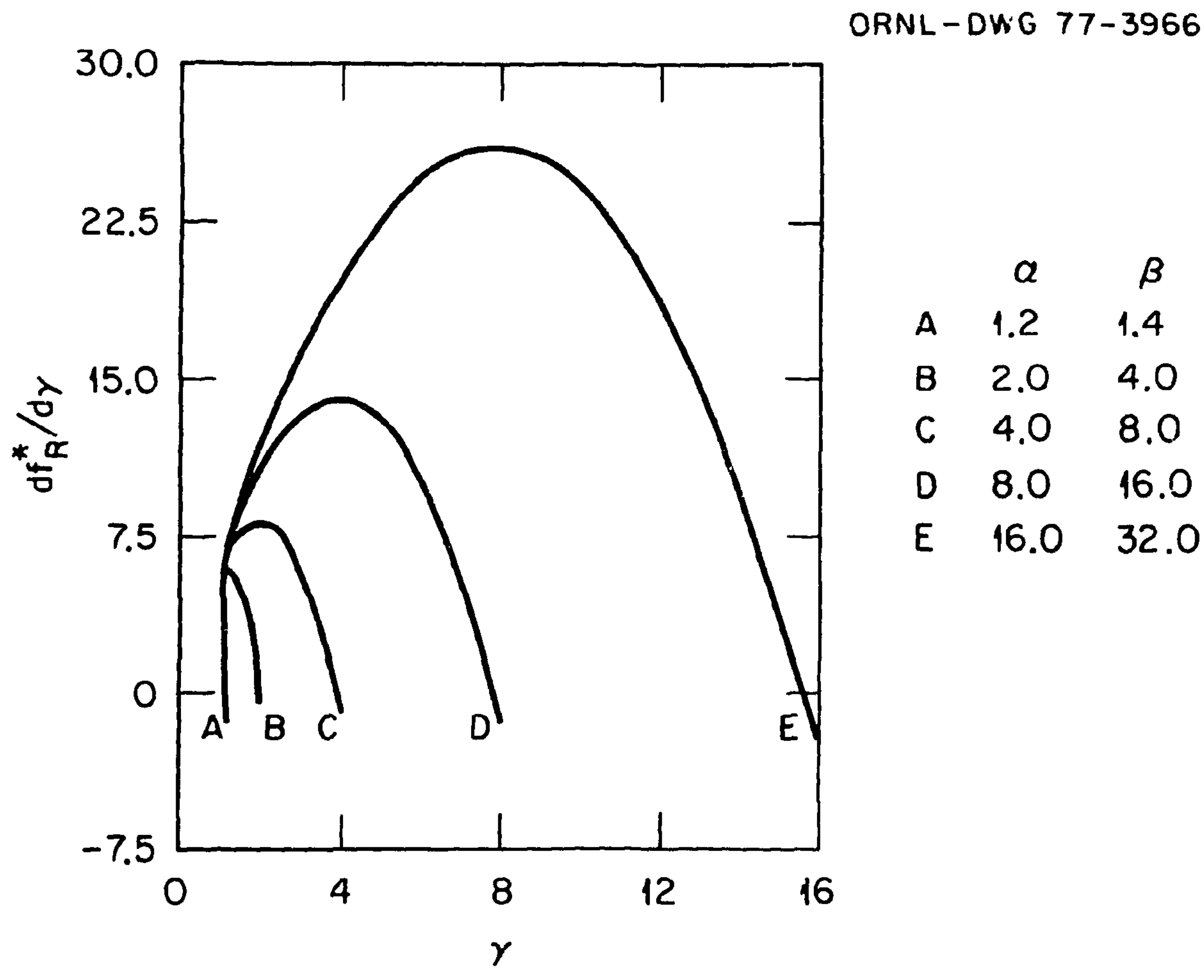

Fig. 16. Change of the normalized body force distribution with respect to position vs nondimensional position for five geometrically different solenoids.

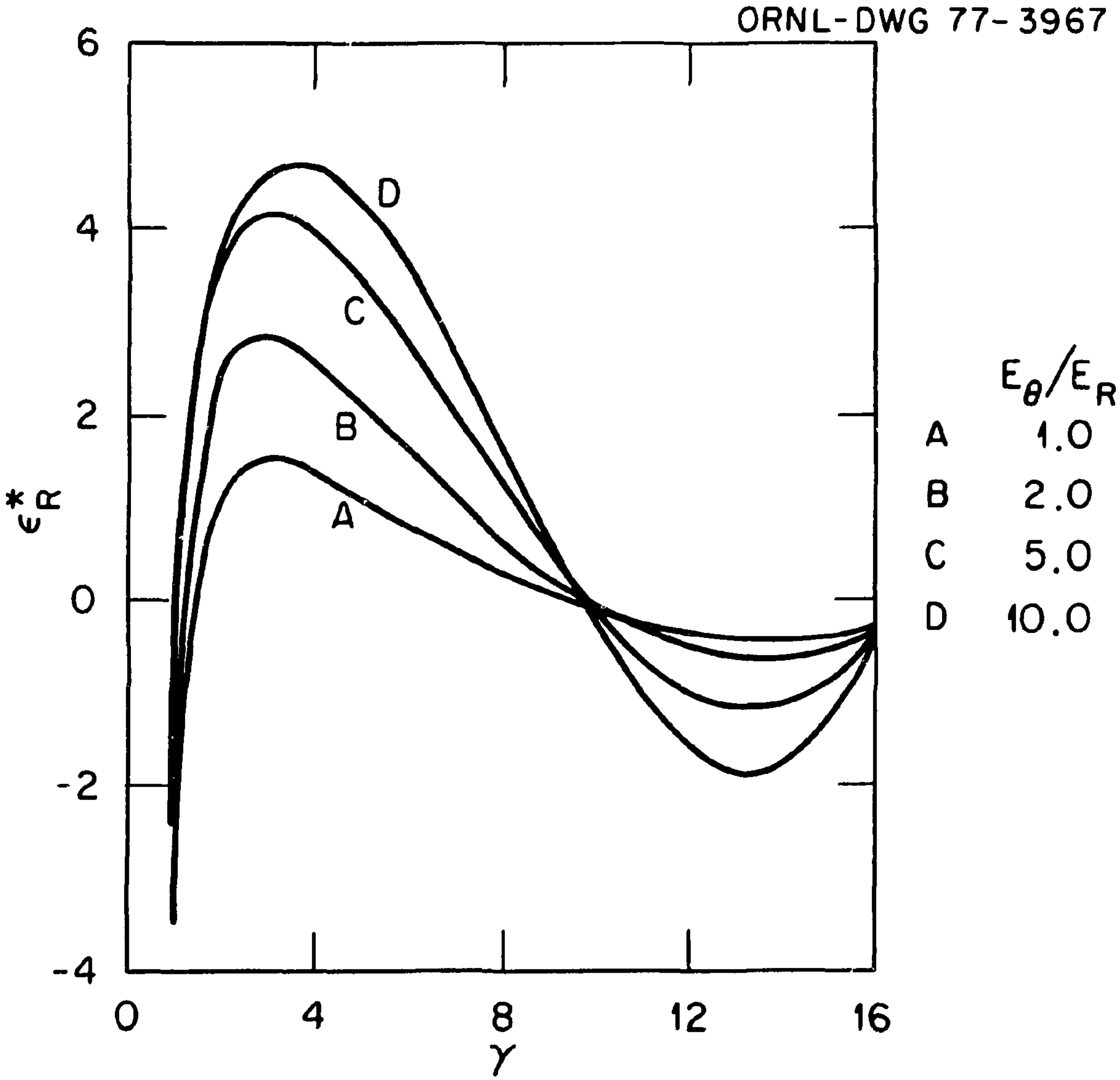

Fig. 17. Nondimensional radial strain versus nondimensional position for four values of transverse isotropy and α = 16.0.

ORNL-DWG 77-3968

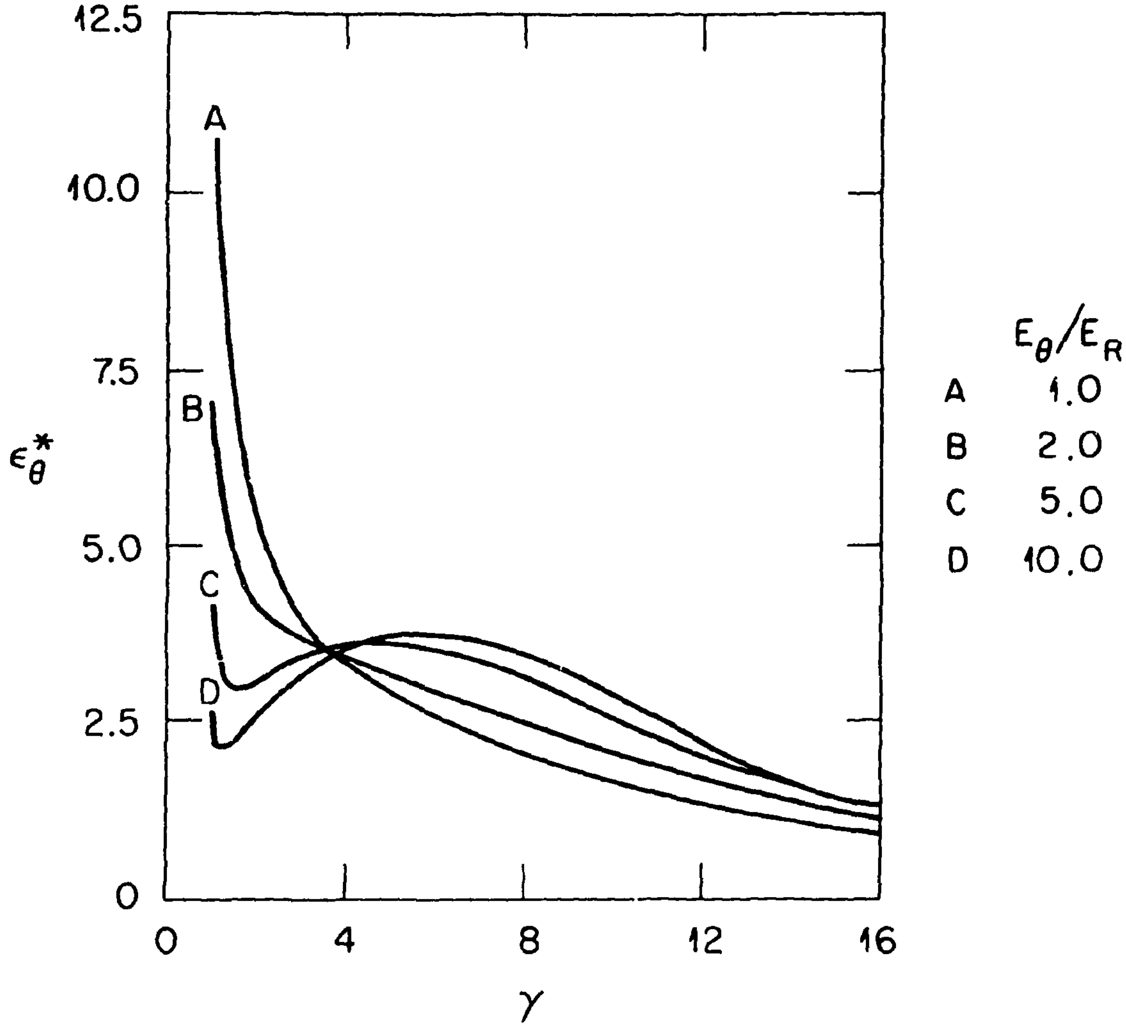

Fig. 18. Nondimensional hoop strain vs nondimensional position for four values of transverse isotropy and α = 16.0.

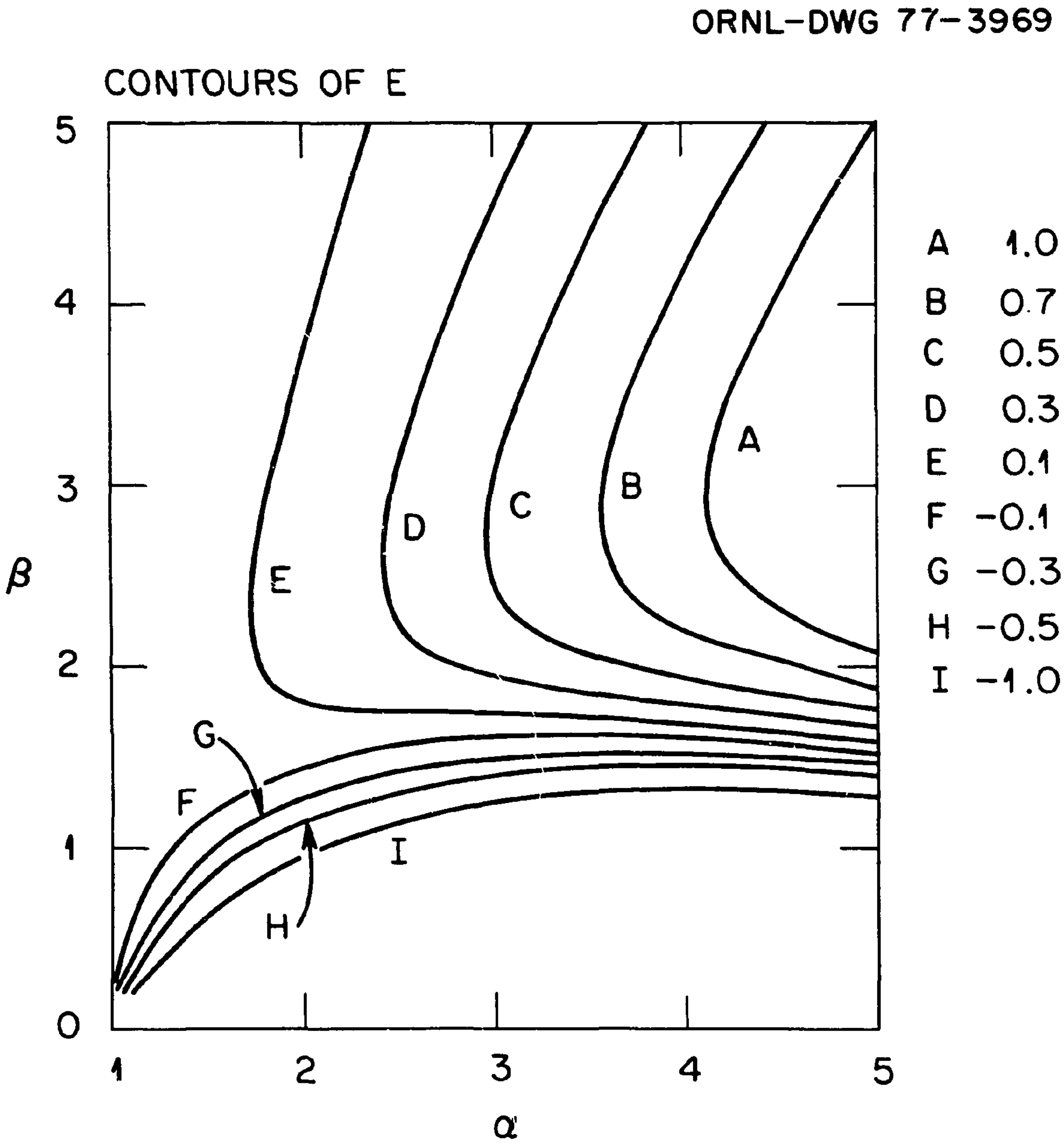

Fig. 19. A contour plot of constant values of the error between F_ℓ and F_m in percent vs α and β for the range $1 \leqslant \alpha \leqslant 5$ and $0.1 \leqslant \beta \leqslant 5$.

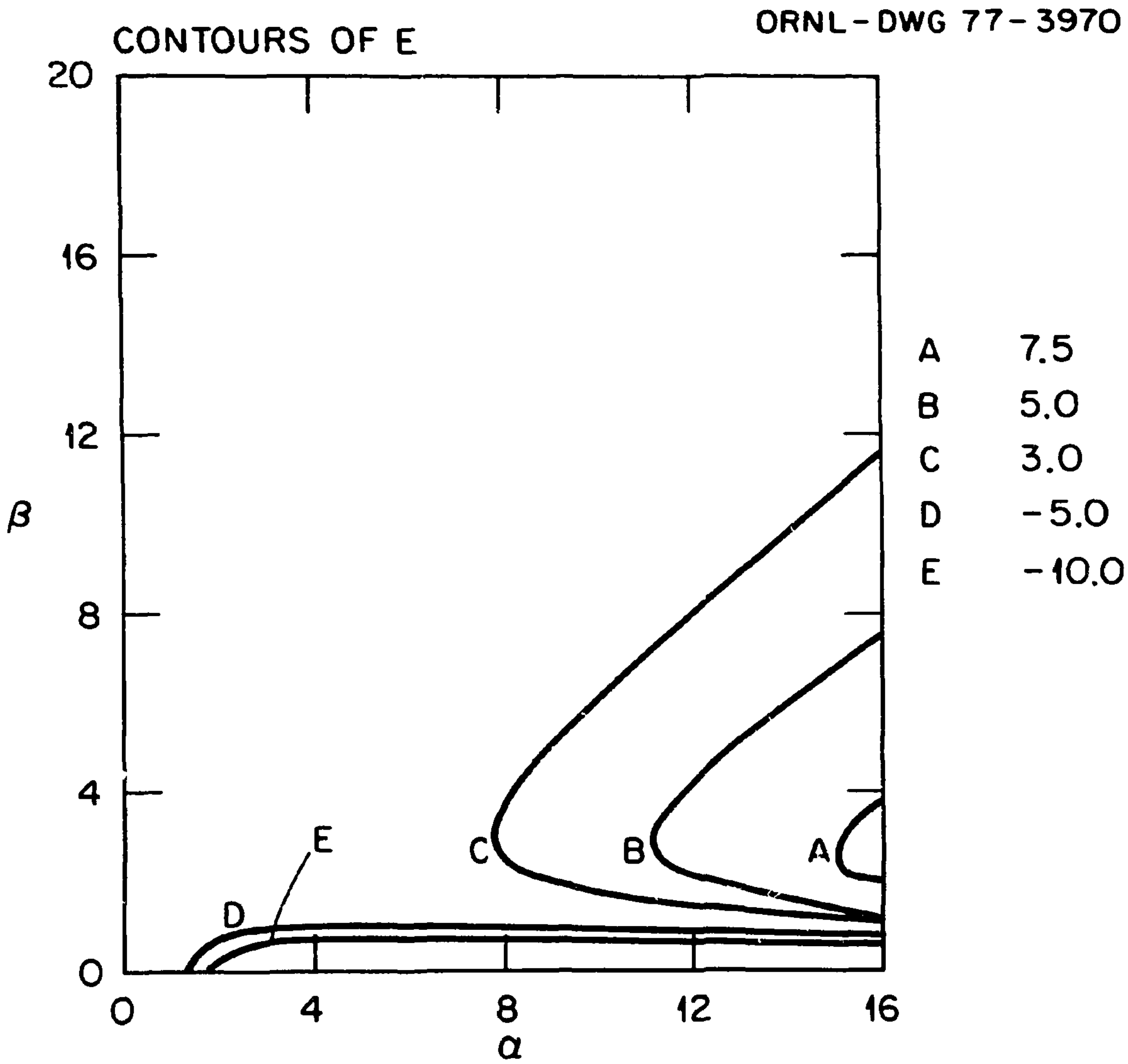

Fig. 20. A contour plot of constant values of the error between F_ℓ and F_m in percent vs α and β for the range $1 \leq \alpha \leq 16$ and $0.1 \leq \beta \leq 20$.

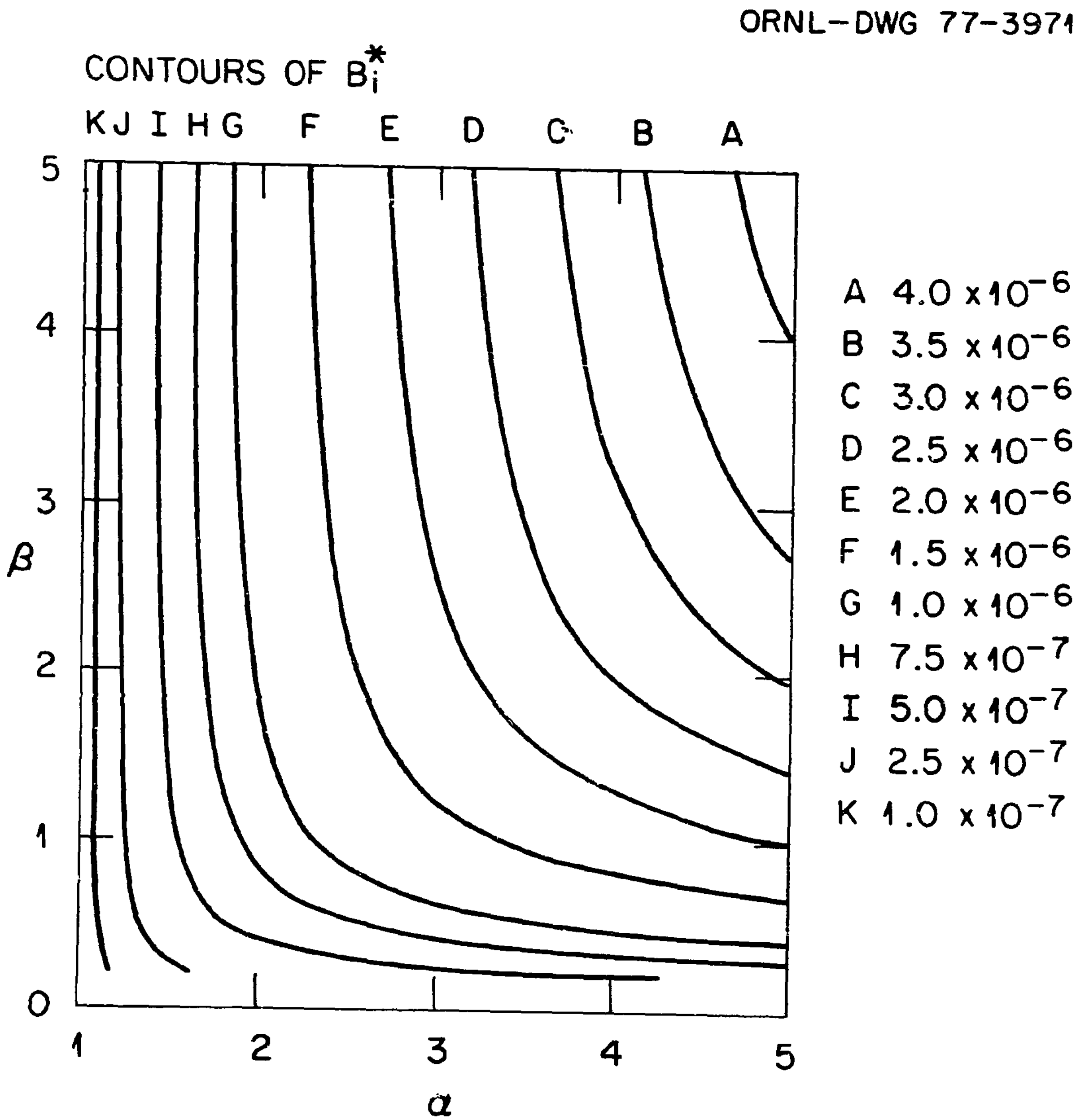

Fig. 21. A contour plot of constant values of the normalized field factor at the inside solenoid radius vs α and β for the range $1 \leq \alpha \leq 5$ and $0.1 \leq \beta \leq 5$.

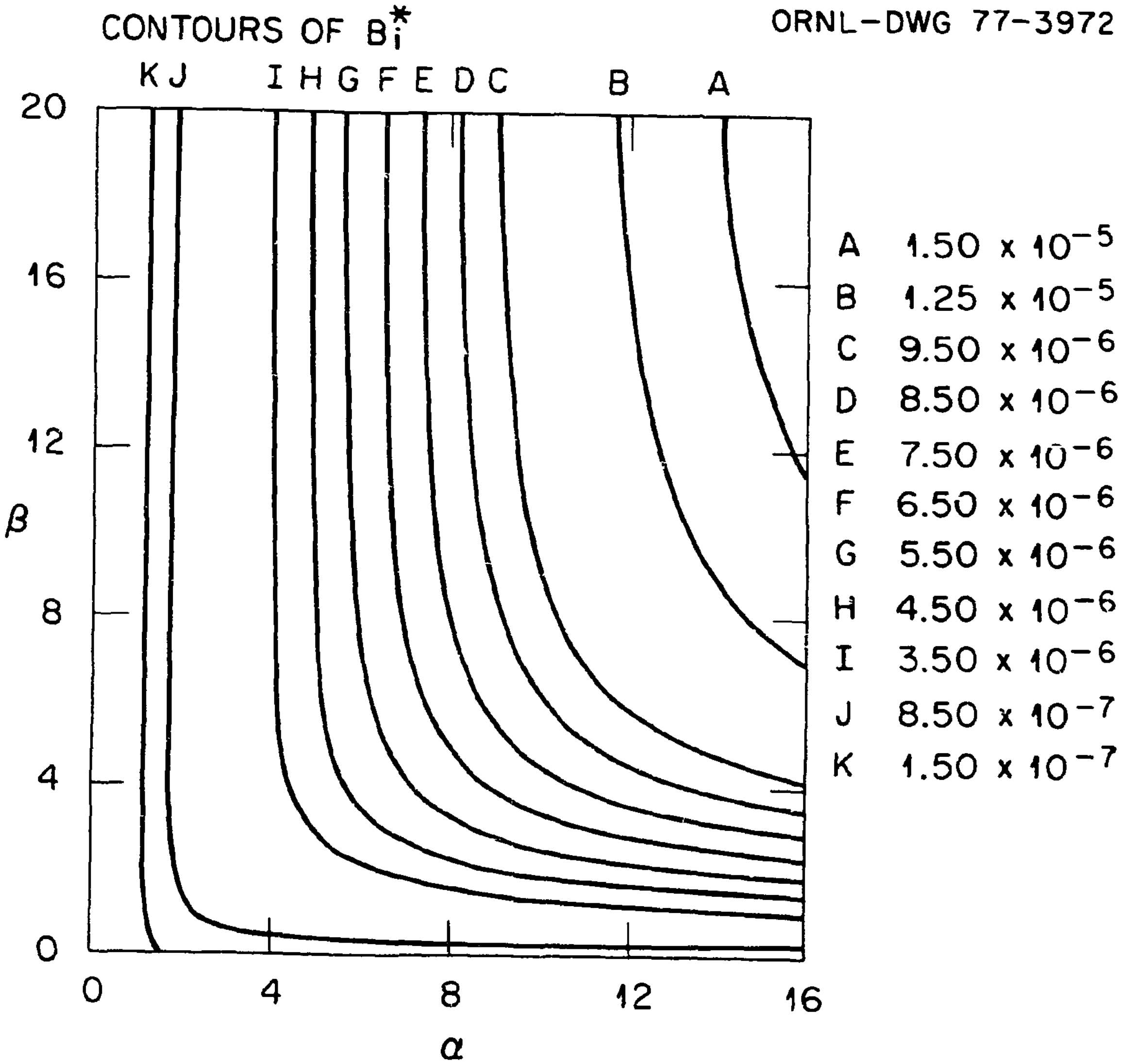

Fig. 22. A contour plot of constant values of the normalized field factor at the inside solenoid radius vs α and β for the range $1 \leqslant \alpha \leqslant 16$ and $0.1 \leqslant \beta \leqslant 20$.

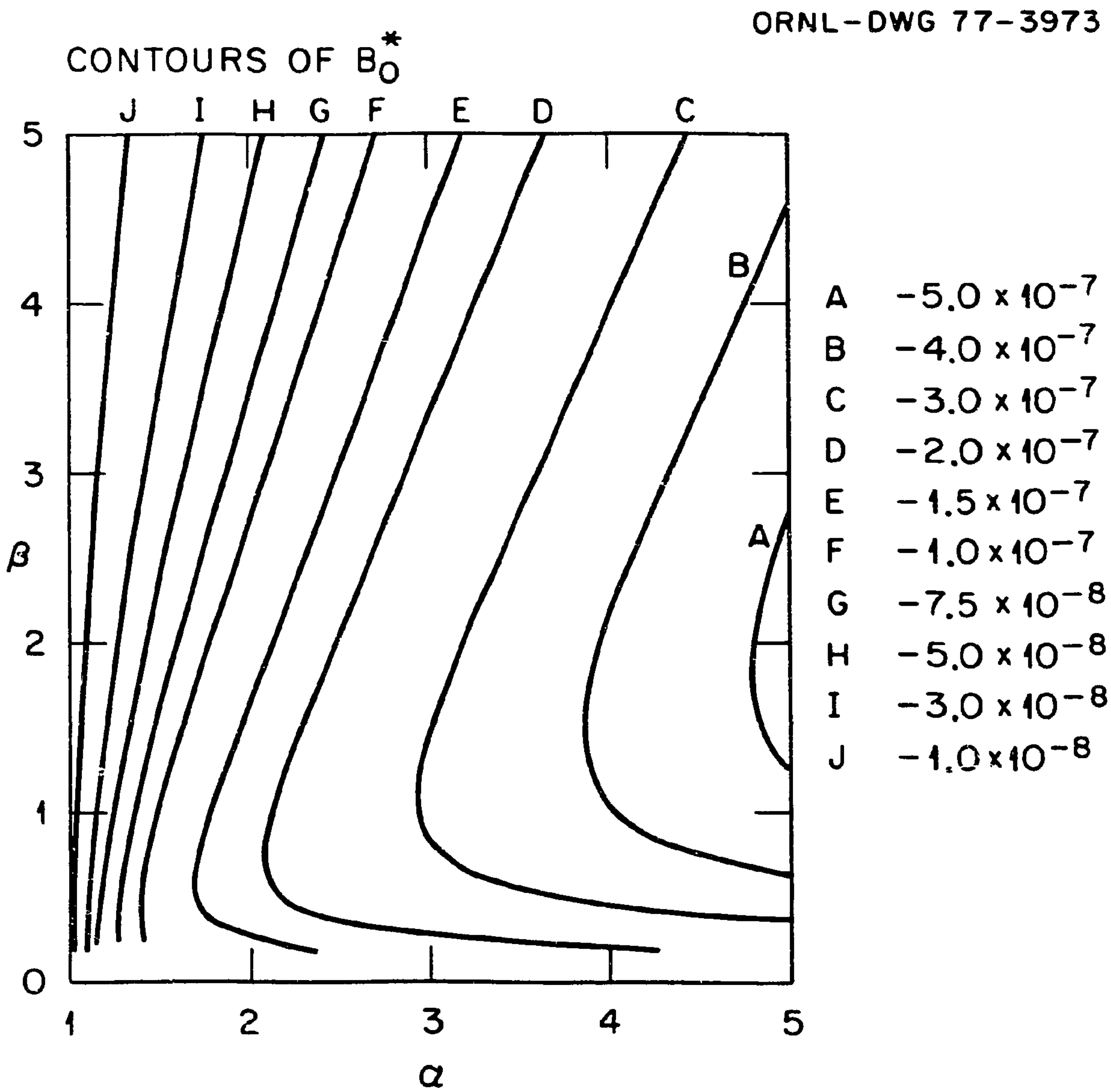

Fig. 23. A contour plot of constant values of the normalized field factor at the outside solenoid radius vs α and β for the range $1 \leqslant \alpha \leqslant 5$ and $0.1 \leqslant \beta \leqslant 5$.

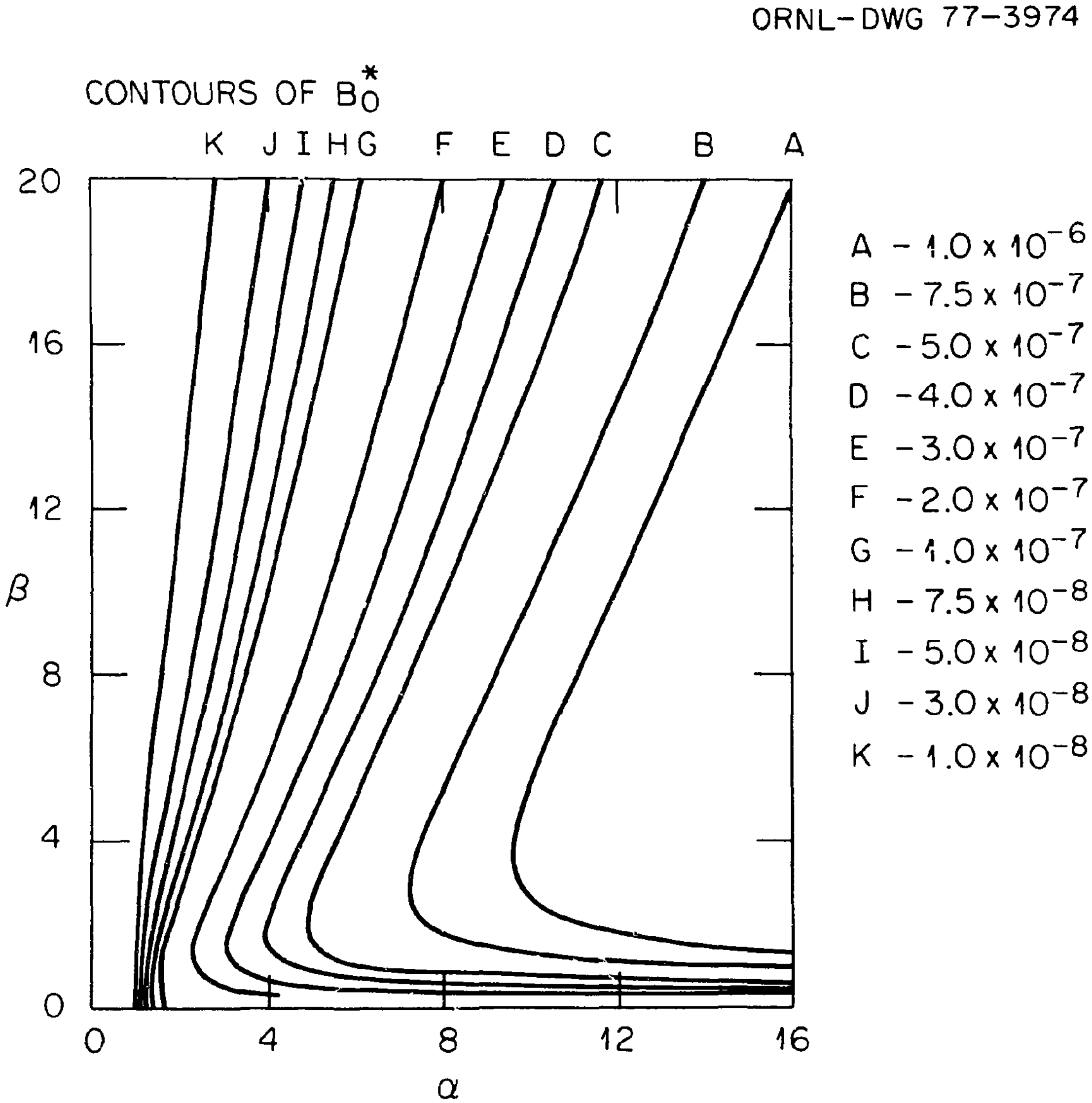

Fig. 24. A contour plot of constant values of the normalized field factor at the outside solenoid radius vs α and β for the range $1 \leqslant \alpha \leqslant 16$ and $0.1 \leqslant \beta \leqslant 20$.

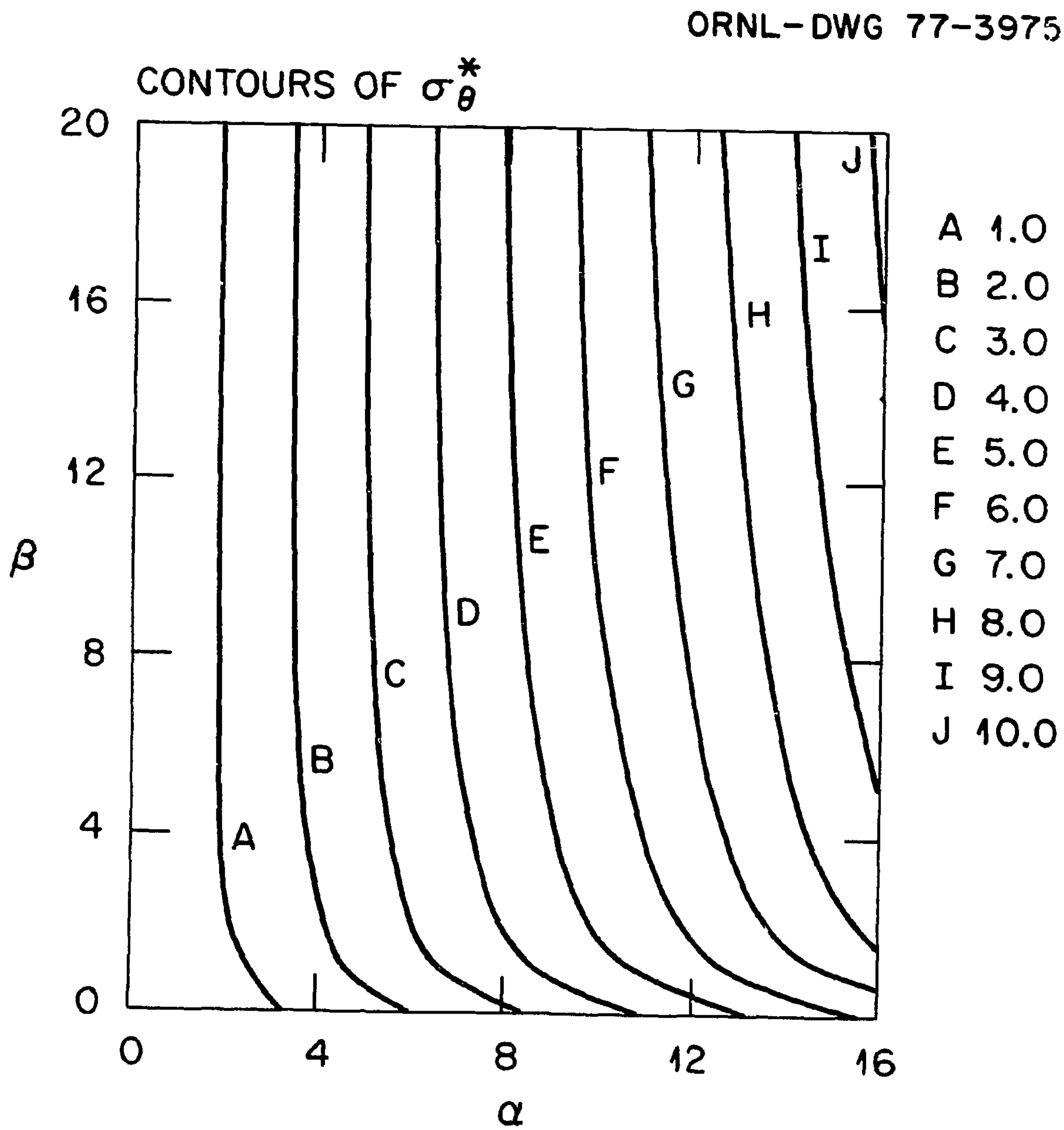

Fig. 25. A contour plot of constant values of the normalized electromechanical hoop stress vs α and β for n = 1.0.

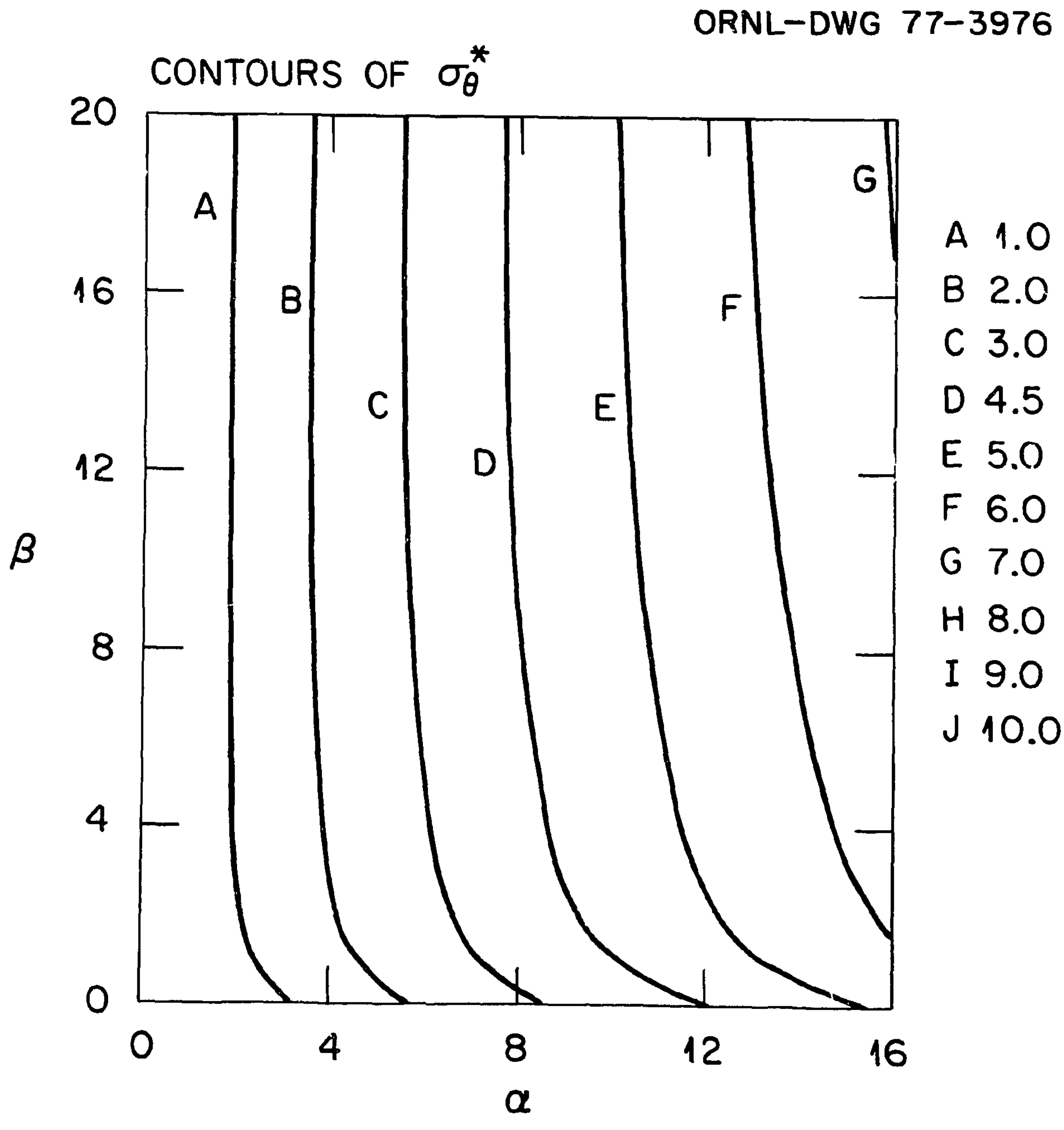

Fig. 26. A contour plot of constant values of the normalized electromechanical hoop stress vs α and β for $n = 2.0$.

ORNL-DWG 77-3977

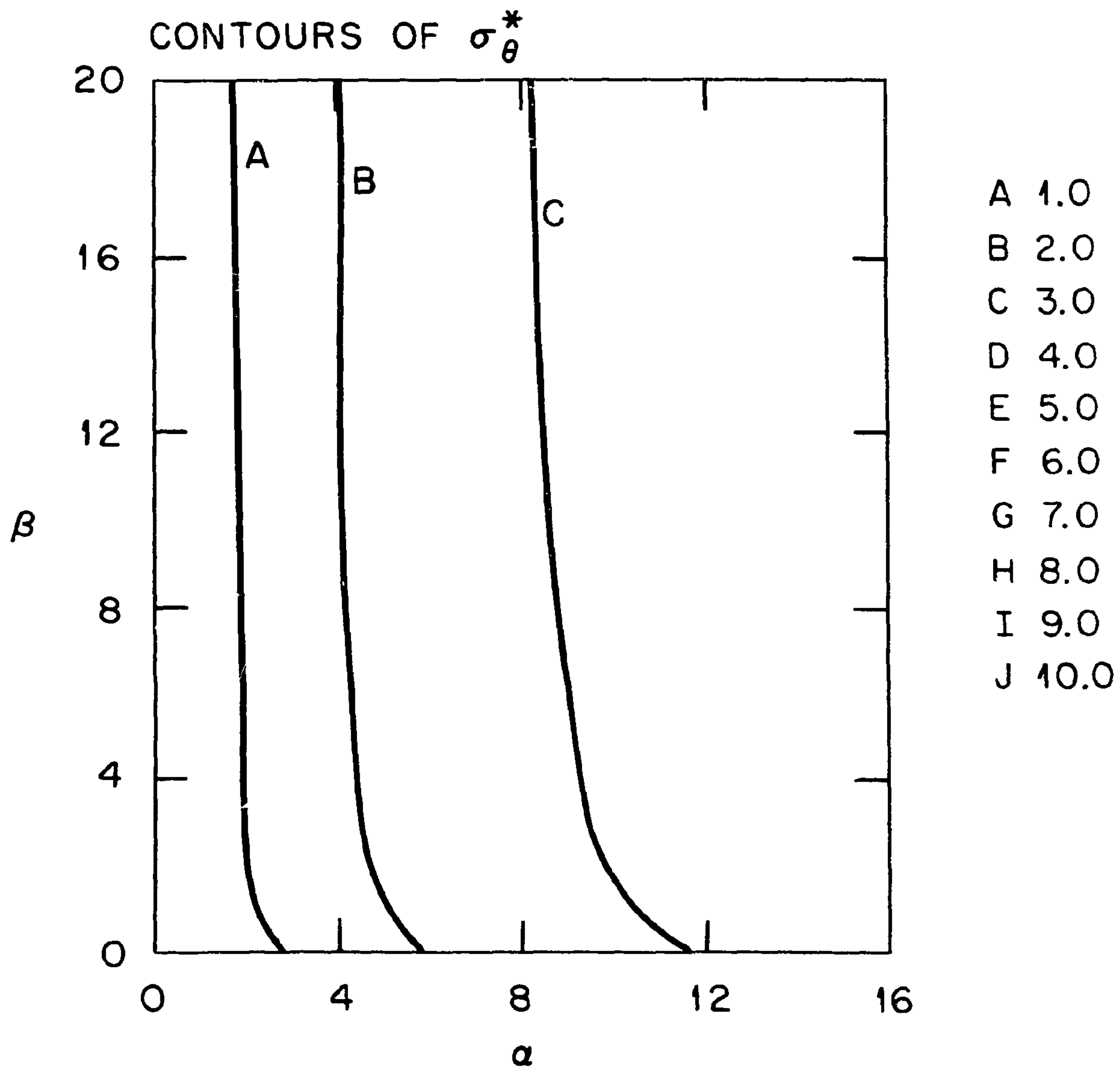

Fig. 27. A contour plot of constant values of the normalized electromechanical hoop stress vs α and β for $n = 5.0$.

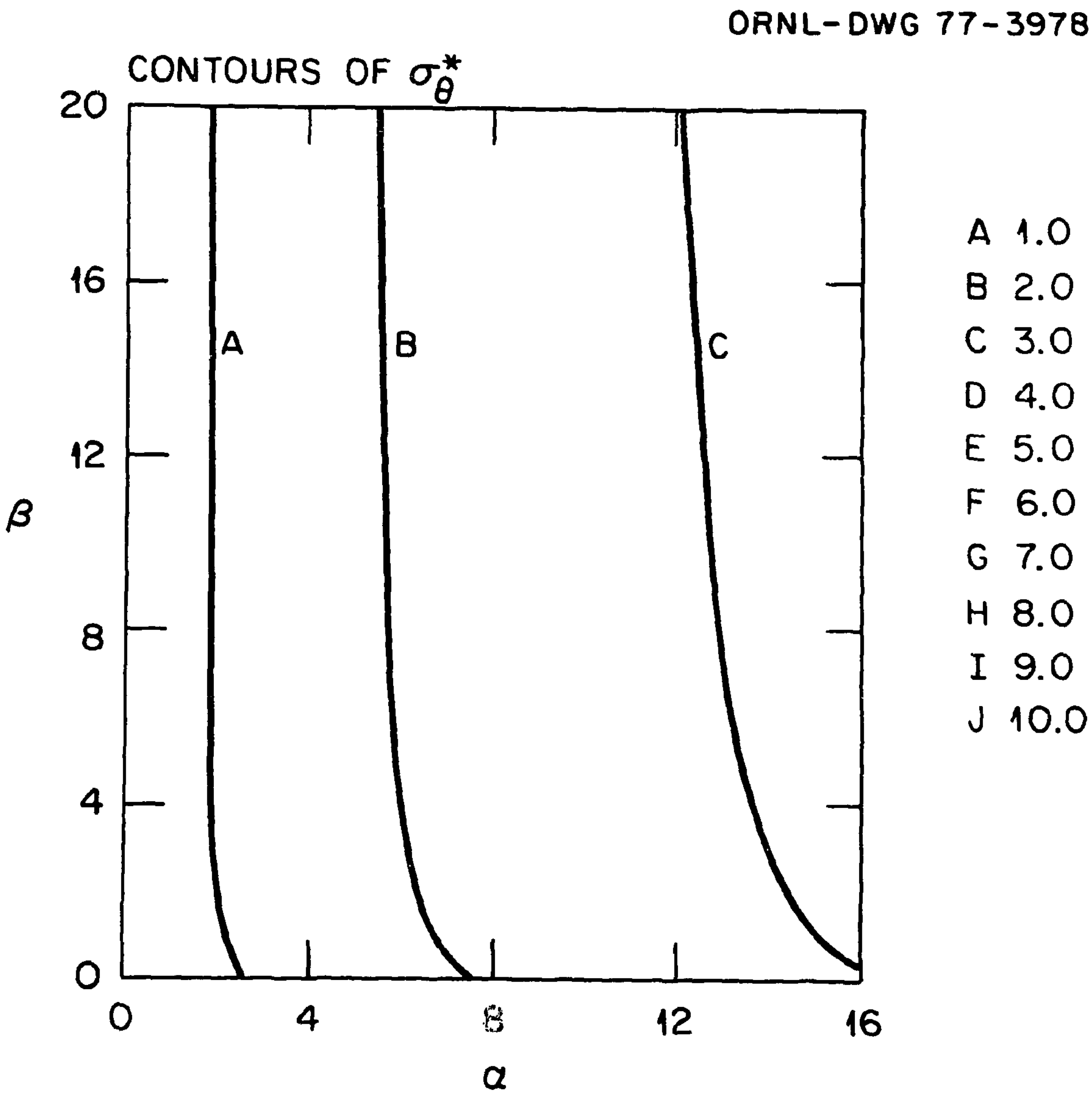

Fig. 28. A contour plot of constant values of the normalized electromechanical hoop stress vs α and β for $n = 10.0$.